

# Star Formation at Very Low Metallicity. IV. Fragmentation Does Not Depend on Metallicity for Cold Initial Conditions.

Anne-Katharina Jappsen<sup>1</sup>

*School of Physics and Astronomy, Cardiff University, Cardiff, UK*

jappsena@cardiff.ac.uk

Ralf S. Klessen

*Institut für Theoretische Astrophysik, Zentrum für Astronomie der Universität Heidelberg,  
Heidelberg, Germany*

rklessen@ita.uni-heidelberg.de

Simon C. O. Glover<sup>2</sup>

*Institut für Theoretische Astrophysik, Zentrum für Astronomie der Universität Heidelberg,  
Heidelberg, Germany*

sglover@ita.uni-heidelberg.de

and

Mordecai-Mark Mac Low<sup>3</sup>

*American Museum of Natural History, New York, NY, USA*

mordecai@amnh.org

## ABSTRACT

Primordial star formation appears to result in stars at least an order of magnitude more massive than modern star formation. It has been proposed that the transition from primordial to modern initial mass functions occurs due to the

---

<sup>1</sup>Formerly at: Canadian Institute for Theoretical Astrophysics, Toronto, ON, Canada

<sup>2</sup>Formerly at: Astrophysikalisches Institut Potsdam, Potsdam, Germany

<sup>3</sup>Also at the Max-Planck-Institut für Astronomie and the Institut für Theoretische Astrophysik, Zentrum für Astronomie der Universität Heidelberg, Heidelberg, Germany

onset of effective metal line cooling at a metallicity  $Z/Z_{\odot} = 10^{-3.5}$ . However, these simulations neglected molecular hydrogen cooling. We perform simulations using the same initial conditions, but including molecular cooling, using a complex network that follows molecular hydrogen formation and also directly follows carbon monoxide and water. We find that molecular hydrogen cooling allows roughly equivalent fragmentation to proceed even at zero metallicity for these initial conditions. The apparent transition just represents the point where metal line cooling becomes more important than molecular cooling. In all cases, the fragments are massive enough to be consistent with models of primordial stellar masses, suggesting that the transition to the modern initial mass function may be determined by other physics such as dust formation. We conclude that such additional cooling mechanisms, combined with the exact initial conditions produced by cosmological collapse are likely more important than metal line cooling in determining the initial mass function, and thus that there is unlikely to be a sharp transition in the initial mass function at  $Z/Z_{\odot} = 10^{-3.5}$ .

*Subject headings:* stars: formation – stars: mass function – early universe – hydrodynamics – equation of state – methods: numerical

## 1. Introduction

The formation of stars is a key process in the early universe with far-reaching consequences for cosmic reionization and galaxy formation (Loeb & Barkana 2001; Bromm & Larson 2004; Glover 2005). The physical processes that govern stellar birth in a metal-free or metal-poor environment, however, are still very poorly understood. Numerical simulations of the thermal and dynamical evolution of gas in primordial protogalactic halos indicate that the metal-free first stars, the so called Population III, are expected to be very massive, with masses anywhere in the range 20–2000  $M_{\odot}$  (Abel, Bryan, & Norman 2002; Bromm et al. 2002; Yoshida *et al.* 2006; O’Shea & Norman 2007). In contrast, the stellar mass spectrum in the present-day universe is dominated by low-mass stars, peaking at around 0.2  $M_{\odot}$  (Scalo 1998; Kroupa 2002; Chabrier 2003). This means that at some stage of cosmic evolution there must have been a transition from primordial, high-mass star formation to the “normal” mode of star formation that dominates today. The discovery of extremely metal-poor subgiant stars in the Galactic halo with masses below one solar mass (Christlieb et al. 2002; Beers & Christlieb 2005) indicates that this transition occurs at abundances considerably smaller than the solar value. At the extreme end, these stars have iron abundances less than  $10^{-5}$  times the solar value, and carbon or oxygen abundances that are still  $\lesssim 10^{-3}$

times the solar value. These stars are thus strongly iron deficient, which could be due to unusual abundance patterns produced by substantial mixing and fallback of ejecta during supernovae explosions of stars with masses between 20-130  $M_{\odot}$  (Umeda & Nomoto 2003) or due to mass transfer from a close binary companion (Ryan et al. 2005; Komiya et al. 2007). There are hints for an increasing binary fraction with decreasing metallicity for these stars (Lucatello et al. 2005).

In a seminal paper, Bromm et al. (2001) proposed that the transition from high to low mass star formation should occur at a critical metallicity  $Z_{\text{crit}} \approx 10^{-3.5} Z_{\odot}$  as a result of atomic fine-structure line cooling from alpha elements, such as carbon and oxygen, becoming important. Their study is based on smoothed particle hydrodynamics simulations of the collapse of cold gas in a top-hat potential at densities below  $n = 10^6 \text{ cm}^{-3}$ . It assumes that cooling from molecular hydrogen is negligible in the density and metallicity range considered. The value of  $Z_{\text{crit}}$  can also be estimated analytically by calculating the metallicity required to produce a cooling rate equal to the rate of adiabatic compression heating for given halo properties (Bromm & Loeb 2003; Santoro & Shull 2006; Frebel, Johnson & Bromm 2007). However, Bromm et al. (2001) noted that neglecting  $\text{H}_2$  cooling could significantly influence the resulting fragmentation pattern. Along the same lines, Omukai et al. (2005) argued, based on the results of detailed one-zone calculations, that molecular cooling would indeed dominate the cooling over many orders of magnitude in density. They argued that dust-induced cooling at densities above  $n \approx 10^{13} \text{ cm}^{-3}$  may be a more viable mechanism to explain fragmentation in very low metallicity gas, a conjecture that has recently been confirmed by Clark et al. (2008).

The effects of molecular cooling at densities up to  $n \approx 500 \text{ cm}^{-3}$  have been discussed by Jappsen et al. (2007, hereafter Paper II) in three-dimensional collapse simulations of warm ionized gas in protogalactic halos for a wide range of environmental conditions. This study used a time-dependent chemical network running alongside the hydrodynamic evolution as described in Glover & Jappsen (2007, hereafter Paper I). The physical motivation was to investigate whether small protogalaxies that formed within the relic HII regions left by neighboring Population III stars could form subsequent generations of stars themselves, or whether the elevated temperatures and fractional ionizations found in these regions suppressed star formation until larger protogalaxies formed. We found in Paper II that molecular hydrogen dominates the cooling of the gas for abundances up to at least  $10^{-2} Z_{\odot}$ . In addition, there was no evidence for fragmentation at densities below  $500 \text{ cm}^{-3}$ .

To understand whether this apparent discrepancy with the Bromm et al. (2001) results comes from including molecular hydrogen cooling or from adopting vastly different initial conditions — here ionized halo gas in a dark matter halo with a NFW density profile

(Navarro et al. 1997), there cold atomic gas in a top-hat halo — we apply our time-dependent chemical network with molecular hydrogen cooling to Bromm et al. (2001)-type initial conditions. Our study is structured as follows. In the next section, §2, we give the details on the numerical set-up and the adopted initial conditions which we summarize in Table 1. In §3 we report our results, and we summarize in §4.

## 2. Numerical Set-Up

To adequately describe star formation in the early universe, it is necessary to follow the cooling and possible fragmentation of the gas in the central regions of dark-matter halos over many orders of magnitude in density. Due to the nonlinear nature of the flow, it is not known in advance where and when gravitational collapse will occur, and consequently stars will form. To compute the time evolution of the system we therefore resort to smoothed particle hydrodynamics (SPH), which is a Lagrangian scheme to solve the equations of hydrodynamics (Benz 1990; Monaghan 1992, 2005) coupled with the a simplified version of the time-dependent network discussed in Glover (2009, hereafter, Paper III). The fluid is represented by an ensemble of particles, and flow quantities are obtained by averaging over an appropriate subset of SPH particles. The method is able to resolve high density contrasts as particles are free to move, and so the particle concentration increases naturally in high-density regions. We use a modified version of the parallel SPH code GADGET (Springel 2005). Once the central parts of a collapsing fragment exceed a density  $n = 10^5 \text{ cm}^{-3}$  we introduce a “sink particle” (Bate et al. 1995; Jappsen et al. 2005), which is able to accrete gas from its surroundings while keeping track of the mass and linear and angular momentum of the infalling material. Replacing collapsing high-density cores by accreting sink particles allows us to follow the dynamic evolution of the system over many local free-fall timescales.

### 2.1. Chemistry and Cooling

The chemical model used in our simulations is based on the detailed model of low-metallicity gas chemistry outlined in Paper III. This model includes cooling both from atomic fine structures lines and also from the molecules  $\text{H}_2$ , HD, CO, OH and  $\text{H}_2\text{O}$ . It was designed to accurately follow the formation and destruction of these molecular species over a wide range of temperatures and densities.

In Paper I, we showed that the neglect of molecular species including metals can be justified in simulations of gravitationally collapsing protogalactic gas provided that  $n <$

$500/t_{\text{char}} \text{ cm}^{-3}$ , where  $t_{\text{char}}$  is the characteristic physical timescale of interest, in Myr. At higher gas densities, molecule formation from metals may become more significant, although its ultimate importance depends on a number of factors, such as the temperature and metallicity of the gas, and the presence (or absence) of an ultraviolet radiation field.

Although our chemical model is capable of accounting for the effects of dust, cosmic rays, and photodissociation by an external radiation field, we omit these complications in the present study.

A full list of the chemical reactions included in the chemical network used in this paper is given in Table 2, along with the corresponding rate coefficients and references to the source of the data. Given these rate coefficients, calculation of the appropriate chemical rates is for the most part straightforward. One minor exception is the case of  $\text{H}_2$  collisional dissociation, which has a rate coefficient that depends on both temperature and density. For the collisional dissociation of  $\text{H}_2$  by  $\text{H}$  or  $\text{H}_2$  (reactions 9 & 10), we calculate the rate coefficients using a function of the form

$$\log k_i = \left( \frac{n/n_{\text{cr}}}{1 + n/n_{\text{cr}}} \right) \log k_{i,\text{h}} + \left( \frac{1}{1 + n/n_{\text{cr}}} \right) \log k_{i,\text{l}}, \quad (1)$$

where  $k_{i,\text{l}}$  and  $k_{i,\text{h}}$  are the low density and high density limits for the collisional dissociation rate due to collisions with species  $i$  (which can be found in Table 2), and where the critical density,  $n_{\text{cr}}$ , is given by

$$\frac{1}{n_{\text{cr}}} = \frac{x_{\text{H}}}{n_{\text{cr,H}}} + \frac{x_{\text{H}_2}}{n_{\text{cr,H}_2}}, \quad (2)$$

where  $n_{\text{cr,H}}$  and  $n_{\text{cr,H}_2}$  are the critical densities in pure atomic gas with an infinitesimally dilute quantity of  $\text{H}_2$  and in pure molecular gas respectively. Temperature dependent fits for  $n_{\text{cr,H}}$  and  $n_{\text{cr,H}_2}$  can be found in Table 2. For the collisional dissociation of  $\text{H}_2$  by  $\text{He}$  (reaction 75), we use a slightly different expression, taken from Dove et al. (1987):

$$\log k_{\text{He}} = \log k_{\text{He,h}} - \frac{(\log k_{\text{He,h}} - \log k_{\text{He,l}})}{1.0 + (n/n_{\text{cr,He}})^{1.09}}. \quad (3)$$

Values for  $k_{\text{He,l}}$ ,  $k_{\text{He,h}}$  and  $n_{\text{cr,He}}$  are given in Table 2.

A referenced list of the thermal processes included in our models is given in Table 3. To compute the  $\text{CO}$  and  $\text{H}_2\text{O}$  rotational and vibrational cooling rates, we use the multi-parameter fitting functions given in Neufeld & Kaufman (1993) and Neufeld, Lepp & Melnick (1995). One of the parameters required is the effective column density  $\tilde{N}(M)$  of each coolant  $M$  (where  $M = \text{CO}$  or  $\text{H}_2\text{O}$ ). We calculate this in our simulations using the expression (Neufeld & Kaufman 1993)

$$\tilde{N}(M) = \frac{n(M)}{|\nabla \cdot \mathbf{v}|}, \quad (4)$$

where  $n(M)$  is the local number density of species  $M$ . The Neufeld & Kaufman (1993) and Neufeld, Lepp & Melnick (1995) treatments assume that only collisions with  $\text{H}_2$  are important in determining the CO or  $\text{H}_2\text{O}$  rotational cooling rates, as is appropriate in a fully molecular gas. However, in metal-poor gas, the  $\text{H}_2$  abundance will often be much smaller than the abundances of atomic hydrogen or atomic helium. We therefore use an effective number density  $n_{\text{eff}}$ , given by (Pavlovski et al. 2002; Smith & Rosen 2003)

$$n_{\text{eff}} = n_{\text{H}_2} + \sqrt{2}n_{\text{H}} + 0.5n_{\text{He}} \quad (5)$$

in place of the  $\text{H}_2$  number density in the Neufeld & Kaufman (1993) and Neufeld, Lepp & Melnick (1995) fitting formulae.

Radiative cooling alone is unable to decrease the temperature of the gas below the cosmic microwave background (CMB) temperature, on simple thermodynamical grounds. We account for this effect in an approximate fashion by using a modified radiative cooling rate in our treatment of the gas thermal energy equation. This modified rate,  $\Lambda_{\text{mod}}(T)$ , is given by

$$\Lambda_{\text{mod}}(T) = \Lambda(T) - \Lambda(T_{\text{CMB}}), \quad (6)$$

where  $\Lambda(T)$  and  $\Lambda(T_{\text{CMB}})$  are the unmodified radiative cooling rates at  $T$  and  $T_{\text{CMB}}$  respectively.

For additional details of our chemical networks and cooling function, please consult Papers I and III; further details of their implementation within Gadget are also given in Paper II and in Jappsen et al. (2008, hereafter Paper V).

## 2.2. Initial Conditions

We model the initial dark matter distribution, following Bromm et al. (2001), as an isolated and roughly spherical overdensity described by the top-hat approximation with small-scale fluctuations with an initial variance of  $\sigma^2 \approx 0.1$  added. We consider a halo virializing at  $z_{\text{vir}} = 30$ , which corresponds to a roughly  $3\sigma$  peak with a total mass of  $2 \times 10^6 M_{\odot}$ , corresponding to  $2 \times 10^5 M_{\odot}$  in baryons. The overdense region has a proper radius of 150 pc. For more details on the set-up of the dark matter and the gas distribution see Bromm et al. (2001).

We carry out numerical experiments with five different metallicities ranging from  $Z = 0$  to  $Z = 0.1 Z_{\odot}$ . Aside from the difference in metallicity, these calculations have identical initial conditions. The simulations were initialized at a redshift  $z = 100$ , with an initial gas temperature  $T_{\text{gas,i}} = 200 \text{ K}$ . To study the effect of resolution we ran simulations with

three different resolutions. Our low resolution simulations, have  $N_{\text{DM}} = 13400$  dark matter particles and  $N_{\text{gas}} = 65536$  gas particles. In these simulations, our numerical resolution of  $M_{\text{res}} = 150 M_{\odot}$  was the same as in Bromm et al. (2001). Our higher resolution simulations with  $N_{\text{DM}} = 107177$  and  $N_{\text{gas}} = 8 \times 10^5$  have mass resolution  $M_{\text{res}} = 12.5 M_{\odot}$ . Finally, our highest resolution simulation has  $N_{\text{DM}} = 4057344$  and  $N_{\text{gas}} = 3.2 \times 10^6$ , so its mass resolution is  $M_{\text{res}} = 3.1 M_{\odot}$ . In all of our simulations, both the dark matter and the gas particles were endowed with the same Hubble expansion and were set in rigid rotation with a spin parameter of 0.05, just as in Bromm et al. (2001).

We also consider a halo virializing at a lower redshift of  $z_{\text{vir}} = 25$ , with a total mass of  $2 \times 10^6 M_{\odot}$ , where the overdense region has a proper radius of 200 pc. We summarize the properties of all of the runs in Table 1, where the runs with halos that collapse at a lower redshift are denoted with ”-C”.

### 3. Results

In each of our calculations the halo contracts rapidly and the gas density increases by several orders of magnitude. A disk-like structure builds up in the very center of each halo with a density of  $n \approx 10^3 \text{ cm}^{-3}$  and a diameter of 10 to 20 pc, as illustrated in Figure 1. The disk mass at the time illustrated is of order  $M_{\text{disk}} \sim 2\text{--}3 \times 10^4 M_{\odot}$ , and so it is well-resolved even in the low resolution simulations. The disk is supported by a combination of thermal pressure and rotation and its growth is fed by material falling in along filaments and sheets. This complex disk provides the background for the small-scale initial density fluctuations to grow, some of which become gravitationally unstable and collapse to form stars. In contrast to the results of Bromm et al. (2001), we find that fragmentation of the disk occurs in all of our simulations, and that there is no evidence for a sharp transition in the initial mass function at  $Z = 10^{-3.5} Z_{\odot}$ .

This result can be understood as follows. Regardless of the metal content,  $\text{H}_2$  line cooling maintains the gas temperature at densities above  $10^3 \text{ cm}^{-3}$  close to the CMB temperature ( $T_{\text{CMB}} = 105 \text{ K}$  at the redshift  $z = 37.5$  considered in Figure 2); even in the primordial case, the gas temperature is within a factor of two of this value. The resulting equation of state is therefore approximately isothermal (at high densities) or softer than isothermal (at low densities). The thermal behavior of the gas is depicted in the left column of Figure 2.

The physical conditions where the equation of state changes from softer than isothermal to isothermal or stiffer, i.e. from a regime where the gas cools with increasing density to one where the temperature remains constant or rises again, imprint a characteristic mass in

the fragmentation process (Jappsen et al. 2005; Larson 2005). Because this fragmentation occurs at approximately the same density and temperature in each simulation, the mass distribution of the fragments does not vary greatly from simulation to simulation. In each of our low resolution simulations, between 16 and 18 fragments are formed, with masses in the range  $10^2 M_\odot \leq M \leq 5 \times 10^3 M_\odot$ . The resulting mass spectra are shown as the solid lines in the right-hand column of Figure 2. For comparison, the thermal Jeans mass for gas with temperature  $T_{\text{gas}} = T_{\text{CMB}}$  is approximately  $2.3 \times 10^3 M_\odot$  at  $n = 10^3 \text{ cm}^{-3}$ , the density above which  $\text{H}_2$  line cooling maintains the gas as approximately isothermal, and  $230 M_\odot$  at  $n = 10^5 \text{ cm}^{-3}$ , the density above which we form sinks. To quantify whether the mass spectra differ significantly, we can use the two-sided Kolmogorov-Smirnov test to determine for each of our low resolution, metal-enriched simulations the probability that the mass spectrum produced is drawn from the same underlying distribution as in the run Z0. We show the corresponding cumulative distribution functions of the clump masses in the top panel of Figure 3. We find probabilities of 0.63, 0.22, 0.99 and 0.11 for runs Z-4, Z-3, Z-2 and Z-1 respectively, indicating that the differences between the fragment mass spectra are in general not statistically significant. We also determine the probabilities for the runs Z-3, Z-2 and Z-1 that the mass spectrum is drawn from the same underlying distribution as in the Z-4 simulation. The probabilities are 0.73, 0.63, 0.5, respectively. This shows that there is no significant change in the clump mass function at  $Z = 10^{-3.5} Z_\odot$ .

In our high resolution simulations, we find a greater degree of fragmentation and a broad fragment mass distribution. However, just as in our low resolution simulations, the mass distribution is dominated by fragments with masses  $M > 100 M_\odot$ . We find very few objects with masses close to our resolution limit of  $12.5 M_\odot$ , and there is no indication from our current results that we are missing a substantial population of objects with masses below this limit. As before, we can compare the fragment mass distributions resulting from our three high-resolution simulations with the K-S test. We show our results in the bottom panel of Figure 3. We find that the probabilities that the fragment mass distributions in runs Z-3-BIG and Z-1-BIG are drawn from the same underlying distribution as in run Z0-BIG are 0.11 and 0.02 respectively, indicating that there is a statistically significant difference. If we compare the runs Z-3-BIG and Z-1-BIG then we determine a probability of 0.93 that their drawn from the same underlying distribution. The run with zero metallicity results in fragments with masses above  $100 M_\odot$ , whereas the runs with metallicity also produce fragments with masses between 50 and  $100 M_\odot$ . Although we see some slight influence from the metal-line cooling, we see no evidence for any low-mass star formation: all of the clumps formed are well-resolved, and have masses consistent with recent determinations of the plausible mass range for Population III stars (see e.g. O’Shea & Norman 2007). We see no indication that metal-line cooling at these temperatures and densities is capable of

producing low-mass stars.

We note that the maximum gas temperature during collapse depends on the metallicity. In the zero-metallicity case, the peak temperature  $T_{\text{peak}}$  reached due to compressional heating during the initial contraction of the gas is  $\sim 6 \times 10^3$  K. As the metallicity increases, however,  $T_{\text{peak}}$  decreases. In particular, the run with  $Z = 0.1 Z_{\odot}$  shows a much smaller peak temperature of  $\sim 10^3$  K. This decrease in  $T_{\text{peak}}$  reflects the growing importance of metal-line cooling in cold gas as the metallicity increases. From Figure 2 it is apparent that the metals begin to affect  $T_{\text{peak}}$  once the metallicity exceeds  $Z = 10^{-3} Z_{\odot}$ . This is a lower threshold than found in Jappsen et al. (2007), but the difference is easily understood as a consequence of the fact that in these simulations we start with cold gas, and that the  $\text{H}_2$  cooling rate of the cold, low-density gas in these simulations is much lower than  $\text{H}_2$  cooling rate in the warm, low-density gas studied in Jappsen et al. (2007). Our threshold of  $Z \sim 10^{-3} Z_{\odot}$  is in reasonable agreement with the Bromm et al. (2001) threshold of  $Z \sim 10^{-3.5} Z_{\odot}$ ; however, the key difference here is that at lower metallicities, the  $\text{H}_2$  alone is sufficient to cool the gas, and the outcome of the fragmentation process has very little dependence on whether the cooling comes from the  $\text{H}_2$  or from the metals.

We also test the hypothesis that the fragment mass spectra of run Z-1-BIG and of the higher resolution run Z-1-BIG2 are drawn from the same distribution and find a probability of 0.98. Since the number of fragments are also quite similar we conclude that our runs Z-1-BIG, Z-3-BIG and Z0-BIG are converged.

In all of our simulations the metal-enriched gas is able to cool to the CMB temperature of approximately 110 K at this redshift (Figure 2). This is also true to within a factor of 2 for the primordial case.  $\text{H}_2$  can act as a coolant for the gas down to a temperature of approximately 200 K, which is close to the CMB temperature at this redshift. Since this could be seen as a reason for the lack of influence of the metals that we find, we perform two runs Z0-BIG-C and Z-1-BIG-C with halos that collapse at a lower redshift  $z = 25$ . In Figure 4 we show the results of these two runs. At a redshift  $z = 25$  the CMB temperature is approximately 71 K and the run Z-1-BIG-C is able to cool down to the CMB temperature due to the combination of efficient metal-line cooling and  $\text{H}_2$  cooling. In the primordial case however the gas is not able to cool at all at this redshift. However, by redshift  $z = 18$ , a substantial amount of the gas is nevertheless able to cool, collapse, and fragment from  $\text{H}_2$  cooling, even though  $\text{H}_2$  cannot cool much below  $\sim 200$  K, and so cannot cool down to the CMB temperature at this redshift. We compare the fragment mass distributions resulting from the primordial and the metal-enriched case with the K-S test. We find that the probability that the fragment mass distributions in runs Z0-BIG-C and Z-1-BIG-C are drawn from the same underlying distribution is 0.11. The probability that runs Z-1-BIG-C

and run Z-1-BIG are drawn from the same underlying distribution is 0.05 (see Figure 3). The fragments of run Z-1-BIG-C have masses down to  $30 M_{\odot}$  whereas the fragments created in run Z-1-BIG have masses above  $50 M_{\odot}$ . In both runs the gas is able to cool down to the CMB temperature due to the combination of metal-line cooling and  $H_2$  cooling. Since the CMB temperature is smaller for the run Z-1-BIG-C, the gas can fragment to smaller masses. This demonstrates that in runs with higher metallicity, where the gas is able to cool down to the CMB temperature, this temperature determines the dynamical behavior (c.f. the similar result found by Smith et al. 2008). Nevertheless, in all of the runs, the fragments have masses that are consistent with the expected masses of Population III stars, and there is no evidence for the formation of low-mass Population II stars.

#### 4. Summary and Conclusion

The current study shows that gas in simulations of the type considered here, with low initial temperature, moderate initial rotation, and a top-hat dark-matter overdensity, will readily fragment into multiple objects with masses above  $30 M_{\odot}$ , regardless of metallicity, provided that enough  $H_2$  is present to cool the gas. Rotation leads to the build-up of massive disk-like structures in these simulations which allow smaller-scale fluctuations to grow and become gravitationally unstable to form protostars. The resulting mass spectrum of fragments peaks at a few hundred solar masses, roughly corresponding to the thermal Jeans mass in the disk-like structure.

Our major conclusion is that the metallicity threshold at  $Z = 10^{-3.5} Z_{\odot}$  reported by Bromm et al. (2001) does not represent a critical metallicity above which gas fragments and below which it does not. Rather, this threshold simply marks the point at which metal-line cooling becomes more important than  $H_2$  cooling at the gas densities and temperatures relevant for fragmentation in the disk. This metallicity threshold only represents a critical metallicity for fragmentation in these simulations if  $H_2$  formation is strongly suppressed or not considered (e.g. Bromm et al. 2001). This scenario may be relevant if the extragalactic UV background is strong (Haiman et al. 2000), although recent work suggests that even in this case, suppression of  $H_2$  formation is less important than previously supposed (Wise & Abel 2007; O’Shea & Norman 2008).

We also find that the mass spectrum of fragments formed in these simulations has very little dependence on the metallicity of the gas. In our low-resolution simulations, many of the fragments are only marginally resolved, but we obtain very similar results from our high-resolution simulations, in which the fragments are well-resolved, suggesting that this lack of influence is real.

We further note that simulations performed by Smith & Sigurdsson (2007) that follow the evolution of cold, metal-enriched gas from cosmological initial conditions until collapse do find tentative evidence for a metallicity threshold at around  $Z = 10^{-3} Z_{\odot}$  that must be surmounted before fragmentation will occur. On the other hand, the simulations presented in Paper V that follow the collapse of hot, initially ionized gas into isolated NFW halos find no evidence for any fragmentation at or above this metallicity. We conclude that the question of whether there is a critical metallicity below which the formation of low-mass stars is impossible remains unresolved. Our current results show no evidence for such a critical metallicity: fragmentation occurs even in our  $Z = 0$  simulation, due only to efficient  $H_2$  cooling, and the mass spectrum of the fragments formed does not appear to differ significantly from those obtained from our higher metallicity simulations.

However, the degree of fragmentation occurring in these simulations appears to be a consequence of the initial conditions chosen: simulations using substantially different initial conditions find very different results (Jappsen et al. 2008; Smith & Sigurdsson 2007). Another example arises if we compare our zero metallicity results with the results of Abel, Bryan, & Norman (2002). These authors use proper cosmological initial conditions and in their simulation only one core forms. Thus the fragmentation in our simulation with primordial gas seems to be a generic outcome of the adopted initial conditions. It is therefore important to consider whether a metallicity threshold appears in simulations with different initial conditions and what the most realistic initial conditions are. To make further progress in understanding the role (if any) that metal-line cooling plays in promoting fragmentation, we need to develop a much better understanding of how metals are initially dispersed into the high-redshift interstellar and intergalactic medium, in order to be able to select the most appropriate initial conditions for our simulations.

Our results call attention to an alternative scenario for the transition to the present-day low-mass IMF. Omukai et al. (2005) stress the importance of dust-induced cooling at high densities, which may become important at metallicities as low as  $Z \approx 10^{-6} - 10^{-5} Z_{\odot}$  depending on the adopted dust model (Schneider et al. 2006). Recent numerical simulations by Clark et al. (2008) support this point of view and predict the existence of low-mass stars and even brown dwarfs with metal abundances of  $\sim 10^{-5}$  the solar value (see also Tsuribe & Omukai 2006).

We acknowledge useful discussions with Tom Abel, Volker Bromm, Paul C. Clark, Kazuyuki Omukai, and Naoki Yoshida, and thank the anonymous referee for valuable feedback. This research was supported in part by the US National Science Foundation under Grants No. PHY05-51164, AST03-07854 and AST08-06558, and by the German Science Foundation (DFG) via the Emmy Noether Program under Grant No. KL1358/1 and via

the Priority Program SFB 439 *Galaxies in the Early Universe*. AKJ acknowledges support by the Human Resources and Mobility Programme of the European Community under the contract MEIF-CT-2006-039569. Computations were performed on the McKenzie cluster at the Canadian Institute for Theoretical Astrophysics. RSK, SCOG and AKJ thank the staff and scholars of the Kavli Institute for Theoretical Physics for their hospitality during the final stages of the preparation of this paper, while M-MML thanks the Deutscher Akademischer Austausch Dienst and the Max-Planck-Gesellschaft for research stipends that helped support this work. Figure 1 was produced using SPLASH, a visualization package for SPH written by Price (2007).

## REFERENCES

- Abel, T., Bryan, G. L., & Norman, M. L. 2002, *Science*, 295, 93
- Abrahamsson, E., Krems, R. V., & Dalgarno, A. 2007, *ApJ*, 654, 1171
- Adams, N. G., & Smith, D. 1976a, *Int. J. Mass Spectrom. Ion. Phys.*, 21, 349
- Adams, N. G., & Smith, D. 1976b, *J. Phys. B.*, 9, 1439
- Adams, N. G., Smith, D., & Grief, D. 1978, *Int. J. Mass Spectrom. Ion. Phys.*, 26, 405
- Adams, N. G., Smith, D., & Millar, T. J., 1984, *MNRAS*, 211, 857
- Adams, N. G., Smith, D., & Paulson, J. F. 1980, *J. Chem. Phys.*, 72, 288
- Aldrovandi, S. M. V. & Pequignot, D. 1973, *A&A*, 25, 137
- Alge, E., Adams, N. G., & Smith, D. 1983, *J. Phys. B*, 16, 1433
- Andreazza, C. M., & Singh, P. D. 1997, *MNRAS*, 287, 287
- Anicich, V. G., Futrell, J. H., Huntress, W. T., & Kim, J. K. 1975, *Int. J. Mass Spectrom. Ion. Phys.*, 18, 63
- Anicich, V. G., Huntress, W. T., & Futrell, J. H. 1976, *Chem. Phys. Lett.*, 40, 233
- Azatyan, V. V., Aleksandrov, E. N., & Troshin A. F. 1975, *Kinet. Catal.*, 16, 306
- Barinovs, G., & van Hemert, M. C. 2006, *ApJ*, 636, 923
- Barlow, S. G. 1984, PhD thesis, Univ. Colorado

- Bate, M. R., Bonnell, I. A., & Price, N. M. 1995, *MNRAS*, 277, 362
- Baulch D. L., Cobos, C. J., Cox, R. A., Esser, C., Frank, P., Just, Th., Kerr, J. A., Pilling, M. J., Troe, J., Walker, R. W., & Warnatz, J. 1992, *J. Phys. Chem. Ref. Data*, 21, 411
- Beers, T. C., & Christlieb, N. 2005, *ARA&A*, 43, 531
- Benz, W. 1990, in *Numerical Modelling of Nonlinear Stellar Pulsations Problems and Prospects*, ed. J. R. Buchler (Dordrecht: Kluwer), 269
- Bodenheimer, P. 1995, *ARA&A*, 33, 199
- Bray, I., Burgess, A., Fursa, D. V., & Tully, J. A. 2000, *A&AS*, 146, 481
- Bromm, V., Larson, R. B. 2004, *ARA&A*, 42, 79
- Bromm, V. & Loeb, A. 2003, *Nature*, 425, 812
- Bromm, V., Ferrara, A., Coppi, P. S., & Larson, R. B. 2001, *MNRAS*, 328, 969
- Bromm, V., Coppi, P. S., & Larson, R. B. 2002, *ApJ*, 564, 23
- Carty, D., Goddard, A., Köhler, S. P. K., Sims, I. R., & Smith, I. W. M. 2006, *J. Phys. Chem. A*, 110, 3101
- Cen, R. 1992, *ApJS*, 78, 341
- Chabrier, G. 2003, *PASP*, 115, 763
- Christlieb, N., Bessell, M. S., Beers, T. C., Gustafsson, B., Korn, A., Barklem, P. S., Karlsson, T., Mizuno-Wiedner, M., Rossi, S. 2002, *Nature*, 419, 904
- Clark, P. C., Glover, S. C. O., Klessen, R. S. 2008, *ApJ*, 672, 757
- Cohen, N., & Westberg, K. R. 1979, *J. Phys. Chem.*, 83, 46
- Cohen, N., & Westberg, K. R. 1983, *J. Phys. Chem. Ref. Data*, 12, 531
- Dalgarno, A., Du, M. L., & You, J. H. 1990, *ApJ*, 349, 675
- Dean, A. J., Davidson, D. F., & Hanson, R. K. 1991, *J. Phys. Chem.*, 95, 183
- Dove, J. E., Rusk, A. C. M., Cribb, P. H., & Martin, P. G. 1987, *ApJ*, 318, 379
- Fairbairn, A. R. 1969, *Proc. R. Soc. London A*, 312, 207

- Federer, W., Villinger, H., Howorka, F., Lindinger, W., Tosi, P., Bassi, D., & Ferguson, E. 1984a, *Phys. Rev. Lett.*, 52, 2084
- Federer, W., Ferguson, E., Tosi, P., Villinger, H., Bassi, D., Howorka, F., Lindinger, W., 1984b, *Contrib.-Symp. At. Surf. Phys.*, eds. Howorka, F., Lindinger, W., Maerk, T. D., (Innsbruck:Austria), p. 141
- Fehsenfeld, F. C. 1976, *ApJ*, 209, 638
- Ferland, G. J., Peterson, B. M., Horne, K., Welsh, W. F., & Nahar, S. N. 1992, *ApJ*, 387, 95
- Field, D., Adams, N. G., & Smith, D. 1980, *MNRAS*, 192, 1
- Frank, P. 1986, *Proc. Int. Symp. Rarefied Gas Dyn.*, 2, 422
- Frank, P., Bhaskaran, K. A., & Just, Th. 1988, *Symp. Int. Combust. Proc.*, 21, 885
- Frank, P., & Just, Th. 1984, *Proc. Int. Symp. Shock Tubes Waves*, 14, 706
- Frebel, A., Johnson, J. L., & Bromm, V. 2007, *MNRAS*, 380, 40
- Geppert, W. D., et al., 2005, *J. Phys.: Conf. Ser.*, 4, 26
- Gerlich, D. 1982, in ‘Symposium on Atomic and Surface Physics’, eds. Lindinger, W., Howorka, F., Märk, T. D., (Dordrecht: Kluwer), p. 304
- Gerlich, D., & Horning, S. 1992, *Chem. Rev.*, 92, 1509
- Glover, S. C. O. 2005, *Space Sci. Reviews*, 117, 445
- Glover, S. C. O. 2009, in preparation. (Paper III)
- Glover, S. C. O., & Jappsen, A.-K. 2007, *ApJ*, 666, 1 (Paper I)
- Guberman, S. L. 1995, *J. Phys. Chem.*, 102, 1699
- Haiman, Z., Abel, T., & Rees, M. J. 2000, *ApJ*, 534, 11
- Harding, L. B., Guadagnini, R., & Schatz, G. C. 1993, *J. Phys. Chem.*, 97, 5472
- Herbst, E. 1985, *ApJ*, 291, 226
- Herbst, E., Millar, T. J., Wlodek, S., & Bohme, D. K. 1989, *A&A*, 222, 205
- Hollenbach, D., McKee, C. F. 1979, *ApJS*, 41, 555

- Hollenbach, D., & McKee, C. F. 1989, *ApJ*, 342, 306
- Hummer, D. G., & Storey, P.J. 1998, *MNRAS*, 297, 1073
- Janev, R. K., Langer, W. D., Evans, K., & Post, D. E. 1987, *Elementary Processes in Hydrogen-Helium Plasmas*, Springer
- Jappsen, A.-K., Klessen, R. S., Larson, R. B., Li, Y., & Mac Low, M.-M. 2005, *A&A*, 435, 611
- Jappsen, A.-K., Glover, S. C. O., Klessen, R. S., & Mac Low, M.-M. 2007, *ApJ*, 660, 1332. (Paper II)
- Jappsen, A.-K., Mac Low, M.-M., Glover, S. C. O., & Klessen, R. S. 2008, *ApJ*, in press; arXiv:0810.1867 (Paper V)
- Jensen, M. J., Bilodeau, R. C., Safvan, C. P., Seiersen, K., Andersen, L. H., Pedersen, H. B., & Heber, O. 2000, *ApJ*, 543, 764
- Jones, J. D. C., Birkinshaw, K., & Twiddy, N. D., 1981, *Chem. Phys. Lett.*, 77, 484
- Karpas, Z., Anicich, V., & Huntress, W. T. 1979, *J. Chem. Phys.*, 70, 2877
- Kim, J. K., Theard, L. P., & Huntress, W. T. 1974, *Int. J. Mass Spectrom. Ion. Phys.*, 15, 223
- Kim, J. K., Theard, L. P., & Huntress, W. T. 1975, *Chem. Phys. Lett.*, 32, 610
- Kimura, M., Dalgarno, A., Chantranupong, L., Li, Y., Hirsch, G., & Buenker, R. J. 1993, *ApJ*, 417, 812
- Kimura, M., Lane, N. F., Dalgarno, A., & Dixon, R. G. 1993, *ApJ*, 405, 801
- Kingdon, J. B. & Ferland, G. J. 1996, *ApJS*, 106, 205
- Komiya, Y., Suda, T., Minaguchi, H., Shigeyama, T., Aoki, W., & Fujimoto, M. Y. 2007, *ApJ*, 658, 367
- Kroupa, P. 2002, *Science*, 295, 82
- Larson, R. B. 2005, *MNRAS*, 359, 211
- Larson, Å., Le Padellec, A., Semaniak, J., Strömholm, C., Larsson, M., Rosén, S., Peverall, R., Danared, H., Djuric, N., Dunn, G. H., & Datz, S. 1998, *ApJ*, 505, 459

- Launay, J. M., Le Dourneuf, M., & Zeippen, C. J. 1991, *A&A*, 252, 842
- Le Boulrot, J., Pineau des Forêts, G., & Flower, D. R. 1999, *MNRAS*, 305, 802
- Lepp, S., & Shull, J. M. 1983, *ApJ*, 270, 578
- Le Teuff, Y. H., Millar, T. J., & Markwick, A. J. 2000, *A&AS*, 146, 157
- Linder, F., Janev, R. K., & Botero, J. 1995, in ‘Atomic and Molecular Processes in Fusion Edge Plasmas’, ed. Janev, R. K., Plenum Press, 397
- Lipovka, A., Núñez-López, R., & Avila-Reese, V. 2005, *MNRAS*, 361, 850
- Loeb, A., Barkana, R. 2001, *ARA&A*, 39, 19
- Lucatello, S., Tsangarides, S., Beers, T. C., Carretta, E., Gratton, R. G., Ryan, S. G. 2005, *ApJ*, 625, 825
- MacGregor, M., & Berry, R. S. 1973, *J. Phys. B*, 6, 181
- Mac Low, M.-M., & Shull, J. M. 1986, *ApJ*, 302, 585
- Martin, P. G., Schwarz, D. H., & Mandy, M. E. 1996, *ApJ*, 461, 265
- Martin, P. G., Keogh W. J., & Mandy, M. E. 1998, *ApJ*, 499, 793
- Mauclaire, G., Deraï, R., & Marx, R. 1978a, *Int. J. Mass Spectrom. Ion. Phys.*, 26, 284
- Mauclaire, G., Deraï, R., & Marx, R. 1978b, *Dyn. Mass Spectrom.*, 5, 139
- Mazzotta, P., Mazzitelli, G., Colafrancesco, S., & Vittorio, N. 1998, *A&AS*, 133, 403
- McCall, B. J., Huneycutt, A. J., Saykally, R. J., Djuric, N., Dunn, G. H., Semaniak, J., Novotny, O., Al-Khalili, A., Ehlerding, A., Hellberg, F., Kalhori, S., Neau, A., Thomas, R. D., Paal, A., Österdahl, F., & Larsson, M. 2004, *Phys. Rev. A*, 70, 052716
- McEwan, M. J., Scott, G. B. I., Adams, N. G., Babcock, L. M., Terzieva, R., & Herbst, E. 1999, *ApJ*, 513, 287
- Mielke, S. L., Lynch, G. C., Truhlar, D. G., & Schwenke, D. W. 1994, *J. Phys. Chem.*, 98, 8000
- Milligan, D. B., & McEwan, M. J. 2000, *Chem. Phys. Lett.*, 319, 482

- Mitchell, J. B. A. 1990, *Phys. Rep.*, 186, 215
- Mitchell, G. F., & Deveau, T. J. 1983, *ApJ*, 266, 646
- Monaghan, J. J. 1992, *ARA&A*, 30, 543
- Monaghan, J. J. 2005, *Rep. Prog. Phys.*, 68, 1703
- Moseley, J., Aberth, W., & Peterson, J. R. 1970, *Phys. Rev. Lett.*, 24, 435
- Murrell, J. N., & Rodriguez, J. A. 1986, *J. Mol. Struct. Theochem.*, 139, 267
- Nahar, S. N. 1995, *ApJS*, 101, 423
- Nahar, S. N. 1996, *ApJS*, 106, 213
- Nahar, S. N. 1999, *ApJS*, 120, 131
- Nahar, S. N. 2000, *ApJS*, 126, 537
- Nahar, S. N. & Pradhan, A. K. 1997, *ApJS*, 111, 339
- Natarajan, K., & Roth, P. 1987, *Combust. Flame*, 70, 267
- Navarro, J. F., Frenk, C. S., & White, S. D. M. 1997, *ApJ*, 490, 493
- Neufeld, D. A., & Kaufman, M. J. 1993, *ApJ*, 418, 263
- Neufeld, D. A., Lepp, S., & Melnick, G. J. 1995, *ApJS*, 100, 132
- Oldenberg, R. C., Loge, G. W., Harradine, D. M., & Winn, K. R. 1992, *J. Phys. Chem*, 96, 8426
- Oh, S. P. & Haiman, Z. 2003, *MNRAS*, 346, 456
- Omukai, K., Tsuribe, T., Schneider, R., & Ferrara, A. 2005, *ApJ*, 626, 627
- Orel, A. E. 1987, *J. Chem. Phys.*, 87, 314
- O’Shea, B. W., & Norman, M. L. 2007, *ApJ*, 654, 66
- O’Shea, B. W., & Norman, M. L. 2008, *ApJ*, 673, 14
- Pavlovski, G., Smith, M. D., Mac Low, M.-M., & Rosen, A. 2002, *MNRAS*, 337, 477
- Peart, B., & Hayton, D. A. 1994, *J. Phys. B*, 27, 2551

- Petuchowski, S. J., Dwek, E., Allen, J. E., Jr., Nuth, III, J. A. 1989, *ApJ*, 342, 406
- Pouilly, B., Robbe, J. M., Schamps, J., & Roueff, E. 1983, *J. Phys. B*, 16, 437
- Poulaert, G., Brouillard, F., Claeys, W., McGowan, J. W., & Van Wassenhove, G. 1978, *J. Phys. B*, 11, L671
- Prasad, S. S., & Huntress, W. T. 1980, *ApJS*, 43, 1
- Price, D. J. 2007, *PASA*, 24, 159
- Raksit, A. B., & Warneck, P. 1980, *J. Chem. Soc. Farad. Trans.*, 76, 1084
- Ramaker, D. E., & Peek, J. M. 1976, *Phys. Rev. A*, 13, 58
- Rosén, S., Peverall, R., Larsson, M., Le Padellec, A., Semaniak, J., Larson, Å., Strömholm, C., van der Zande, W. J., Danared, H., & Dunn, G. H. 1998, *Phys. Rev.*, 57, 4462
- Rosén, S., Derkatch, A. M., Semaniak, J., Neau, A., Al-Khalili, A., Le Padellec, A., Viktor, L., Thomas, R., Danared, H., af Ugglas, M., & Larsson, M. 2000, *Faraday Discuss.*, 115, 295
- Ryan, S. G., Aoki, W., Norris, J. E., & Beers, T. C. 2005, *ApJ*, 635, 349
- Saigo, K., Matsumoto, T., & Hanawa, T. 2000, *ApJ*, 531, 971
- Santoro, F. & Shull, J. M. 2006, *ApJ*, 643, 26
- Savin, D. W. 2002, *ApJ*, 566, 599
- Savin, D. W., Krstic, P. S., Haiman, Z., & Stancil, P. C. 2004, *ApJ*, 606, L167; erratum *ApJ*, 607, L147
- Scalo, J. 1998, in *ASP Conf. Ser. 142: The Stellar Initial Mass Function*, ed. G. Gilmore & D. Howell (San Francisco: Astron. Soc. Pac.), 201
- Schneider, I. F., Dulieu, O., Giusti-Suzor, A., & Roueff, E. 1994, *ApJ*, 424, 983; erratum *ApJ*, 486, 580
- Schneider, R., Omukai, K., Inoue, A. K., & Ferrara, A. 2006, *MNRAS*, 369, 1437
- Shapiro, P. R., & Kang, H. 1987, *ApJ*, 318, 32
- Shavitt, I. 1959, *J. Chem. Phys.*, 31, 1359

- Sidhu, K. S., Miller, S., & Tennyson, J. 1992, *A&A*, 255, 453
- Singh, P. D., Sanzovo, G. C., Borin, A. C., & Ornellas, F. R. 1999, *MNRAS*, 303, 235
- Slack, M. W., 1976, *J. Chem. Phys.*, 64, 228
- Smith, B. S., Sigurdsson, S. 2007, *ApJ*, 661, L5
- Smith, B. D., Turk, M. J., Sigurdsson, S., O’Shea, B. W., & Norman, M. L. 2008, *ApJ*, in press; arXiv:0806.1653
- Smith, D., & Adams, N. G. 1977a, *Int. J. Mass Spectrom. Ion. Phys.*, 23, 123
- Smith, D., & Adams, N. G. 1977b, *Chem. Phys. Lett.*, 47, 383
- Smith, D., Adams, N. G., & Miller, T. M. 1978, *J. Chem. Phys.*, 69, 308
- Smith, I. W. M., Herbst, E., & Chang, Q. 2004, *MNRAS*, 350, 323
- Smith, M. D., & Rosen, A. 2003, *MNRAS*, 339, 133
- Smith, M. A., Schlemmer, S., von Richthofen, J., & Gerlich, D. 2002, *ApJ*, 578, L87
- Smith, D., Spanel, P., & Mayhew, C. A. 1992, *Int. J. Mass Spectrom. Ion. Proc.*, 117, 457
- Spergel, D. N., Verde, L., Peiris, H. V., et al. 2003, *ApJS*, 148, 175
- Springel, V. 2005, *MNRAS*, 364, 1105
- Stancil, P. C., & Dalgarno, A. 1998, *Far. Disc.*, 109, 61
- Stancil, P. C., Havener, C. C., Krstic, P. S., Schultz, D. R., Kimura, M., Gu, J.-P., Hirsch, G., Buenker, R. J., & Zygelman, B. 1998, *ApJ*, 502, 1006
- Stancil, P. C., Schultz, D. R., Kimura, M., Gu, J.-P., Hirsch, G., & Buenker, R. J. 1999, *A&AS*, 140, 225
- Stancil, P. C., Kirby, K., Gu, J.-P., Hirsch, G., Buenker, R. J., & Sannigrahi, A. B. 2000, *A&AS*, 142, 107
- Stibbe, D. T., & Tennyson, J. 1999, *ApJ*, 513, L147
- Takagi, H., Kosugi, N., & Le Dourneuf, M. 1991, *J. Phys. B*, 24, 711
- Tominaga, N., Umeda, H., & Nomoto, K. 2007, *ApJ*, 660, 516

- Tsang, W., & Hampson, R. F. 1986, *J. Phys. Chem. Ref. Data*, 15, 1087
- Tsuribe, T., & Omukai, K. 2006, *ApJ*, 642, L61
- Umeda, H., & Nomoto, K. 2003, *Nature*, 422, 871
- Viggiano, A. A., Howorka, F., Albritton, D. L., Fehsenfeld, F. C., Adams, N. G., & Smith, D. 1980, *ApJ*, 236, 492
- Voronov, G. S. 1997, *ADNDT*, 65, 1
- Wagner-Redeker, W., Kemper, P. R., Jarrold, M. F., & Bowers, M. T., 1985, *J. Chem. Phys.*, 83, 1121
- Walkauskas, L. P., & Kaufman, F. 1975, *Symp. Int. Combust. Proc.*, 15, 691
- Warnatz, J. 1984, in ‘Combustion Chemistry’, ed. W. C. Gardiner, Jr., (Springer-Verlag:NY), 197
- Watson, W. D., Anicich, V. G., & Huntress, W. T. 1976, *ApJ*, 205, L165
- Wise, J. H., & Abel, T. 2007, *ApJ*, 671, 1559
- Wishart, A. W. 1979, *MNRAS*, 187, 59P
- Woodall, J., Agúndez, M., Markwick-Kemper, A. J., & Millar, T. J., 2007, *A&A*, 466, 1197
- Yoshida, N., Omukai, K., Hernquist, L., & Abel, T. 2006, *ApJ*, 652, 6
- Zhao, L. B., Stancil, P. C., Gu, J. P., Liebermann, H.-P., Li, Y., Funke, P., Buenker, R. J., Zygelman, B., Kimura, M., & Dalgarno, A. 2004, *ApJ*, 615, 1063
- Zygelman, B., Dalgarno, A., Kimura, M., & Lane, N. F. 1989, *Phys. Rev. A*, 40, 2340

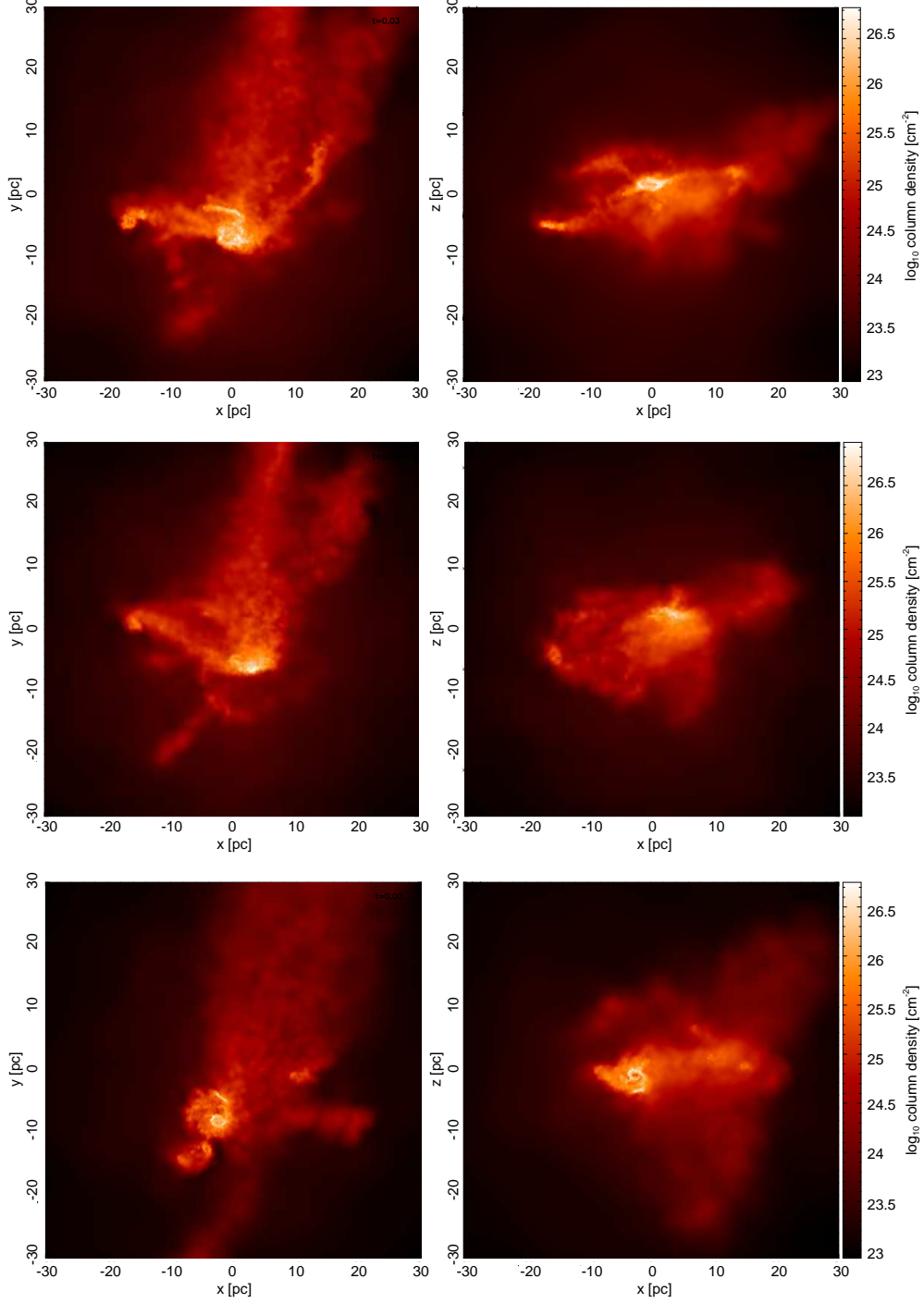


Fig. 1.— *From top to bottom:* Projected gas number density in runs Z0, Z-3, and Z-1 at  $z = 35$ . *Left:* Face-on view. *Right:* Edge-on view. The size of the box is 60 pc.

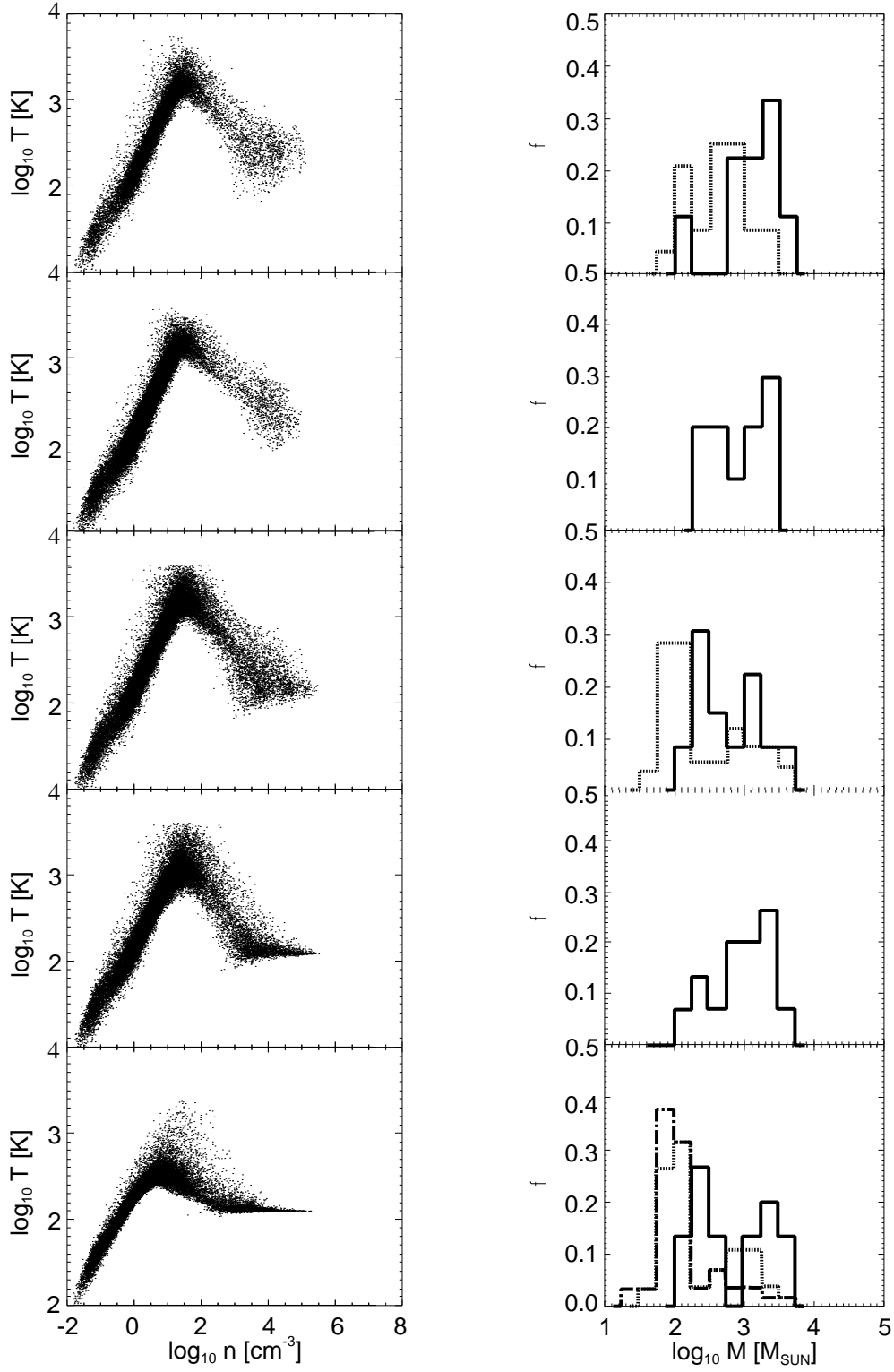


Fig. 2.— *From top to bottom*: Gas properties and mass distribution of clumps at  $z = 37.5$  for runs Z0, Z-4, Z-3, Z-2, and Z-1, arranged in order of increasing metallicity. *Left*: Temperature versus number density of the gas. *Right*: Mass distribution of the clumps represented by sink particles. In the panels for runs Z0, Z-3, and Z-1 we also show the results for the higher resolution runs Z0-BIG, Z-3-BIG, and Z-1-BIG (*dotted lines*). The *dot-dashed line* in the bottom panel represents the run with the highest resolution Z-1-BIG2.

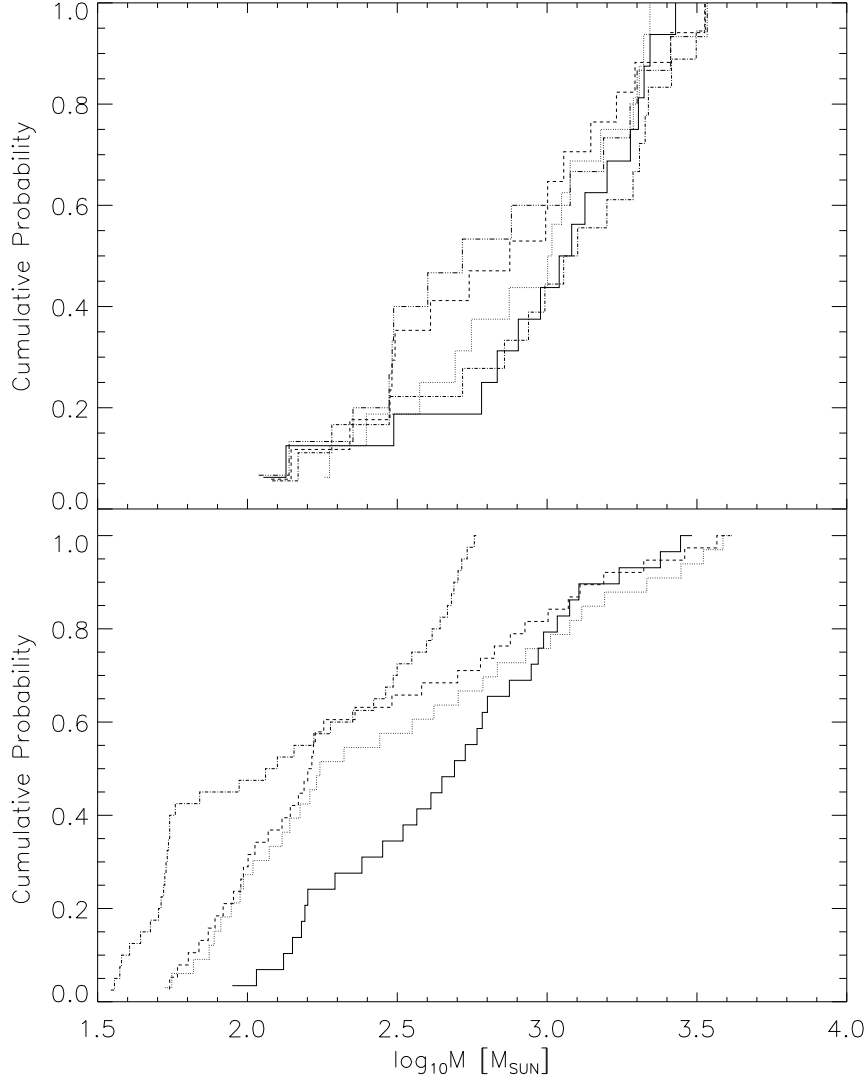


Fig. 3.— *Top panel:* Cumulative distribution function of the clump masses for the low resolution runs Z0 (*solid line*), Z-4 (*dotted line*), Z-3 (*dashed line*), Z-2 (*dot-dashed line*), and Z-1 (*dot-dot-dashed line*). *Bottom panel:* Cumulative distribution function of the clump masses for the higher resolution runs Z0-BIG (*solid line*), Z-3-BIG (*dotted line*), Z-1-BIG (*dashed line*) and Z-1-BIG-C (*dot-dashed line*).

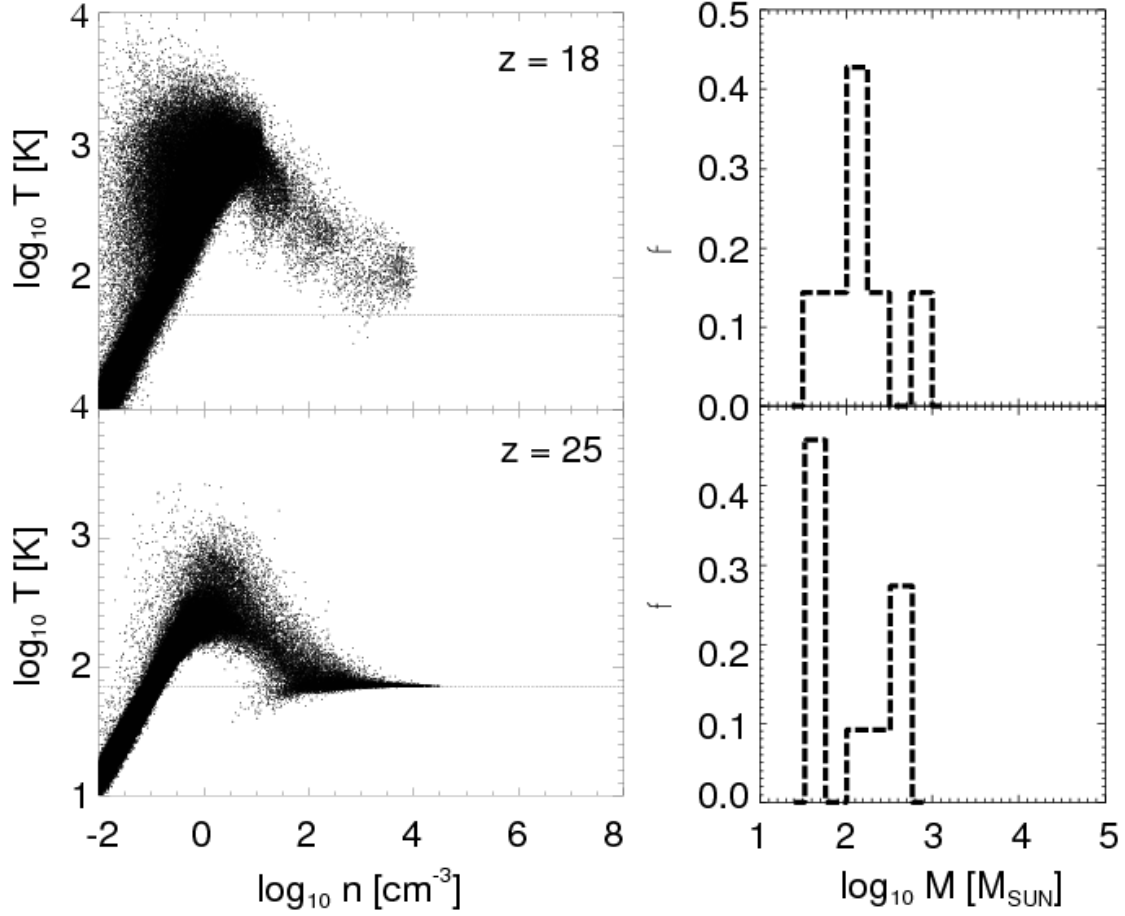


Fig. 4.— *Top panel:* Gas properties and mass distribution of clumps at  $z = 18$  for the run Z0-BIG-C. In this run no clumps have formed yet at  $z = 25$  when the halo starts to collapse. *Bottom panel:* Gas properties and mass distribution of clumps at  $z = 25$  for the run Z-1-BIG-C. The *dashed line* shows the CMB temperature.

Table 1. List of the runs discussed in this paper

Run	$Z^{\text{a}}$ ( $Z_{\odot}$ )	$\lambda^{\text{b}}$	$N_{\text{gas}}^{\text{c}}$	$N_{\text{clump}}^{\text{d}}$
Z0	0.0	0.05	65536	16
Z-4	$10^{-4}$	0.05	65536	16
Z-3	$10^{-3}$	0.05	65536	17
Z-2	$10^{-2}$	0.05	65536	18
Z-1	$10^{-1}$	0.05	65536	17
Z0-BIG	0.0	0.05	$8 \times 10^5$	29
Z-3-BIG	$10^{-3}$	0.05	$8 \times 10^5$	33
Z-1-BIG	$10^{-1}$	0.05	$8 \times 10^5$	38
Z-1-BIG2	$10^{-1}$	0.05	$3.2 \times 10^6$	38
Z0-BIG-C	0.0	0.05	$8 \times 10^5$	32
Z-1-BIG-C	$10^{-1}$	0.05	$8 \times 10^5$	40

<sup>a</sup>Metallicity of the gas.

<sup>b</sup>Spin parameter of the halo.

<sup>c</sup>Number of SPH particles representing the gas.

<sup>d</sup>Number of clumps at  $z = 18.0$  for the runs marked with ”-C” and for all other runs at  $z = 37.5$ .

Table 2. List of reactions in our chemical model.

No.	Reaction	Rate coefficient (cm <sup>3</sup> s <sup>-1</sup> )	Ref.
1	$\text{H} + \text{e}^- \rightarrow \text{H}^- + \gamma$	$k_1 = \text{dex}[-17.845 + 0.762 \log T + 0.1523(\log T)^2$ $\quad - 0.03274(\log T)^3]$ $= \text{dex}[-16.420 + 0.1998(\log T)^2$ $\quad - 5.447 \times 10^{-3}(\log T)^4$ $\quad + 4.0415 \times 10^{-5}(\log T)^6]$	<div style="display: flex; justify-content: space-between;"> <span><math>T \leq 6000 \text{ K}</math></span> <span>1</span> </div> <div style="display: flex; justify-content: space-between;"> <span><math>T &gt; 6000 \text{ K}</math></span> <span></span> </div>
2	$\text{H}^- + \text{H} \rightarrow \text{H}_2 + \text{e}^-$	$k_2 = 1.5 \times 10^{-9}$ $= 4.0 \times 10^{-9} T^{-0.17}$	<div style="display: flex; justify-content: space-between;"> <span><math>T \leq 300 \text{ K}</math></span> <span>2</span> </div> <div style="display: flex; justify-content: space-between;"> <span><math>T &gt; 300 \text{ K}</math></span> <span></span> </div>
3	$\text{H} + \text{H}^+ \rightarrow \text{H}_2^+ + \gamma$	$k_3 = \text{dex}[-19.38 - 1.523 \log T$ $\quad + 1.118(\log T)^2 - 0.1269(\log T)^3]$	3
4	$\text{H} + \text{H}_2^+ \rightarrow \text{H}_2 + \text{H}^+$	$k_4 = 6.4 \times 10^{-10}$	4
5	$\text{H}^- + \text{H}^+ \rightarrow \text{H} + \text{H}$	$k_5 = 5.7 \times 10^{-6} T^{-0.5} + 6.3 \times 10^{-8}$ $\quad - 9.2 \times 10^{-11} T^{0.5} + 4.4 \times 10^{-13} T$	5
6	$\text{H}_2^+ + \text{e}^- \rightarrow \text{H} + \text{H}$	$k_6 = 1.0 \times 10^{-8}$ $= 1.32 \times 10^{-6} T^{-0.76}$	<div style="display: flex; justify-content: space-between;"> <span><math>T \leq 617 \text{ K}</math></span> <span>6</span> </div> <div style="display: flex; justify-content: space-between;"> <span><math>T &gt; 617 \text{ K}</math></span> <span></span> </div>
7	$\text{H}_2 + \text{H}^+ \rightarrow \text{H}_2^+ + \text{H}$	$k_7 = [-3.3232183 \times 10^{-7}$ $\quad + 3.3735382 \times 10^{-7} \ln T$ $\quad - 1.4491368 \times 10^{-7} (\ln T)^2$ $\quad + 3.4172805 \times 10^{-8} (\ln T)^3$ $\quad - 4.7813720 \times 10^{-9} (\ln T)^4$ $\quad + 3.9731542 \times 10^{-10} (\ln T)^5$ $\quad - 1.8171411 \times 10^{-11} (\ln T)^6$ $\quad + 3.5311932 \times 10^{-13} (\ln T)^7]$ $\times \exp\left(\frac{-21237.15}{T}\right)$	7
8	$\text{H}_2 + \text{e}^- \rightarrow \text{H} + \text{H} + \text{e}^-$	$k_8 = 3.73 \times 10^{-9} T^{0.1121} \exp\left(\frac{-99430}{T}\right)$	8
9	$\text{H}_2 + \text{H} \rightarrow \text{H} + \text{H} + \text{H}$	$k_{9,1} = 6.67 \times 10^{-12} T^{1/2} \exp\left[-\left(1 + \frac{63590}{T}\right)\right]$	9
		$k_{9,h} = 3.52 \times 10^{-9} \exp\left(-\frac{43900}{T}\right)$	10

Table 2—Continued

No.	Reaction	Rate coefficient (cm <sup>3</sup> s <sup>-1</sup> )	Ref.
		$n_{\text{cr,H}} = \text{dex} \left[ 3.0 - 0.416 \log \left( \frac{T}{10000} \right) - 0.327 \left\{ \log \left( \frac{T}{10000} \right) \right\}^2 \right]$	10
10	$\text{H}_2 + \text{H}_2 \rightarrow \text{H}_2 + \text{H} + \text{H}$	$k_{10,\text{l}} = \frac{5.996 \times 10^{-30} T^{4.1881}}{(1.0 + 6.761 \times 10^{-6} T)^{5.6881}} \exp \left( -\frac{54657.4}{T} \right)$	11
		$k_{10,\text{h}} = 1.3 \times 10^{-9} \exp \left( -\frac{53300}{T} \right)$	12
		$n_{\text{cr,H}_2} = \text{dex} \left[ 4.845 - 1.3 \log \left( \frac{T}{10000} \right) + 1.62 \left\{ \log \left( \frac{T}{10000} \right) \right\}^2 \right]$	12
11	$\text{H} + \text{e}^- \rightarrow \text{H}^+ + \text{e}^- + \text{e}^-$	$k_{11} = \exp[-3.271396786 \times 10^1$ $+ 1.35365560 \times 10^1 \ln T_e$ $- 5.73932875 \times 10^0 (\ln T_e)^2$ $+ 1.56315498 \times 10^0 (\ln T_e)^3$ $- 2.87705600 \times 10^{-1} (\ln T_e)^4$ $+ 3.48255977 \times 10^{-2} (\ln T_e)^5$ $- 2.63197617 \times 10^{-3} (\ln T_e)^6$ $+ 1.11954395 \times 10^{-4} (\ln T_e)^7$ $- 2.03914985 \times 10^{-6} (\ln T_e)^8]$	13
12	$\text{D} + \text{e}^- \rightarrow \text{D}^+ + \text{e}^- + \text{e}^-$	$k_{12} = k_{11}$	—
13	$\text{H}^+ + \text{e}^- \rightarrow \text{H} + \gamma$	$k_{13,\text{A}} = 1.269 \times 10^{-13} \left( \frac{315614}{T} \right)^{1.503}$ $\times [1.0 + \left( \frac{604625}{T} \right)^{0.470}]^{-1.923}$ $k_{13,\text{B}} = 2.753 \times 10^{-14} \left( \frac{315614}{T} \right)^{1.500}$ $\times [1.0 + \left( \frac{115188}{T} \right)^{0.407}]^{-2.242}$	Case A 14 Case B 14
14	$\text{D}^+ + \text{e}^- \rightarrow \text{D} + \gamma$	$k_{14} = k_{13}$	—
15	$\text{H}^- + \text{e}^- \rightarrow \text{H} + \text{e}^- + \text{e}^-$	$k_{15} = \exp[-1.801849334 \times 10^1$ $+ 2.36085220 \times 10^0 \ln T_e$ $- 2.82744300 \times 10^{-1} (\ln T_e)^2$ $+ 1.62331664 \times 10^{-2} (\ln T_e)^3$ $- 3.36501203 \times 10^{-2} (\ln T_e)^4$ $+ 1.17832978 \times 10^{-2} (\ln T_e)^5$ $- 1.65619470 \times 10^{-3} (\ln T_e)^6$ $+ 1.06827520 \times 10^{-4} (\ln T_e)^7$ $- 2.63128581 \times 10^{-6} (\ln T_e)^8]$	13

Table 2—Continued

No.	Reaction	Rate coefficient (cm <sup>3</sup> s <sup>-1</sup> )		Ref.
16	H <sup>-</sup> + H → H + H + e <sup>-</sup>	$k_{16} = 2.5634 \times 10^{-9} T_{\text{e}}^{1.78186}$ $= \exp[-2.0372609 \times 10^1$ $+ 1.13944933 \times 10^0 \ln T_{\text{e}}$ $- 1.4210135 \times 10^{-1} (\ln T_{\text{e}})^2$ $+ 8.4644554 \times 10^{-3} (\ln T_{\text{e}})^3$ $- 1.4327641 \times 10^{-3} (\ln T_{\text{e}})^4$ $+ 2.0122503 \times 10^{-4} (\ln T_{\text{e}})^5$ $+ 8.6639632 \times 10^{-5} (\ln T_{\text{e}})^6$ $- 2.5850097 \times 10^{-5} (\ln T_{\text{e}})^7$ $+ 2.4555012 \times 10^{-6} (\ln T_{\text{e}})^8$ $- 8.0683825 \times 10^{-8} (\ln T_{\text{e}})^9]$	$T_{\text{e}} \leq 0.1 \text{ eV}$  $T_{\text{e}} > 0.1 \text{ eV}$	13
17	H <sup>-</sup> + H <sup>+</sup> → H <sub>2</sub> <sup>+</sup> + e <sup>-</sup>	$k_{17} = 6.9 \times 10^{-9} T^{-0.35}$ $= 9.6 \times 10^{-7} T^{-0.90}$	$T \leq 8000 \text{ K}$ $T > 8000 \text{ K}$	15
18	H + D <sup>+</sup> → D + H <sup>+</sup>	$k_{18} = 2.06 \times 10^{-10} T^{0.396} \exp\left(-\frac{33}{T}\right)$ $+ 2.03 \times 10^{-9} T^{-0.332}$		16
19	D + H <sup>+</sup> → H + D <sup>+</sup>	$k_{19} = 2.0 \times 10^{-10} T^{0.402} \exp\left(-\frac{37.1}{T}\right)$ $- 3.31 \times 10^{-17} T^{1.48}$ $= 3.44 \times 10^{-10} T^{0.35}$	$T \leq 2 \times 10^5 \text{ K}$  $T > 2 \times 10^5 \text{ K}$	16
20	H <sub>2</sub> + D <sup>+</sup> → HD + H <sup>+</sup>	$k_{20} = [0.417 + 0.846 \log T - 0.137(\log T)^2] \times 10^{-9}$		17
21	HD + H <sup>+</sup> → H <sub>2</sub> + D <sup>+</sup>	$k_{21} = 1.1 \times 10^{-9} \exp\left(-\frac{488}{T}\right)$		17
22	H <sub>2</sub> + D → HD + H	$k_{22} = 1.69 \times 10^{-10} \exp\left(-\frac{4680}{T}\right)$ $= 1.69 \times 10^{-10} \exp\left(-\frac{4680}{T} + \frac{198800}{T^2}\right)$	$T \leq 200 \text{ K}$ $T > 200 \text{ K}$	18
23	HD + H → D + H <sub>2</sub>	$k_{23} = 5.25 \times 10^{-11} \exp\left(-\frac{4430}{T}\right)$ $= 5.25 \times 10^{-11} \exp\left(-\frac{4430}{T} + \frac{173900}{T^2}\right)$	$T \leq 200 \text{ K}$ $T > 200 \text{ K}$	19
24	He + e <sup>-</sup> → He <sup>+</sup> + e <sup>-</sup> + e <sup>-</sup>	$k_{24} = \exp[-4.409864886 \times 10^1$ $+ 2.391596563 \times 10^1 \ln T_{\text{e}}$ $- 1.07532302 \times 10^1 (\ln T_{\text{e}})^2$		13

Table 2—Continued

No.	Reaction	Rate coefficient (cm <sup>3</sup> s <sup>-1</sup> )		Ref.
		$+ 3.05803875 \times 10^0 (\ln T_e)^3$ $- 5.6851189 \times 10^{-1} (\ln T_e)^4$ $+ 6.79539123 \times 10^{-2} (\ln T_e)^5$ $- 5.0090561 \times 10^{-3} (\ln T_e)^6$ $+ 2.06723616 \times 10^{-4} (\ln T_e)^7$ $- 3.64916141 \times 10^{-6} (\ln T_e)^8]$		
25	$\text{He}^+ + \text{e}^- \rightarrow \text{He} + \gamma$	$k_{25,\text{rr,A}} = 10^{-11} T^{-0.5} [12.72 - 1.615 \log T$ $- 0.3162 (\log T)^2 + 0.0493 (\log T)^3]$	Case A	20
		$k_{25,\text{rr,B}} = 10^{-11} T^{-0.5} [11.19 - 1.676 \log T$ $- 0.2852 (\log T)^2 + 0.04433 (\log T)^3]$	Case B	20
		$k_{25,\text{di}} = 1.9 \times 10^{-3} T^{-1.5} \exp\left(-\frac{473421}{T}\right)$ $\times [1.0 + 0.3 \exp\left(-\frac{94684}{T}\right)]$		21
26	$\text{He}^+ + \text{H} \rightarrow \text{He} + \text{H}^+$	$k_{26} = 1.25 \times 10^{-15} \left(\frac{T}{300}\right)^{0.25}$		22
27	$\text{He} + \text{H}^+ \rightarrow \text{He}^+ + \text{H}$	$k_{27} = 1.26 \times 10^{-9} T^{-0.75} \exp\left(-\frac{127500}{T}\right)$ $= 4.0 \times 10^{-37} T^{4.74}$	$T \leq 10000 \text{ K}$ $T > 10000 \text{ K}$	23
28	$\text{He}^+ + \text{D} \rightarrow \text{He} + \text{D}^+$	$k_{28} = k_{26}$		—
29	$\text{He} + \text{D}^+ \rightarrow \text{He}^+ + \text{D}$	$k_{29} = k_{27}$		—
30	$\text{C}^+ + \text{e}^- \rightarrow \text{C} + \gamma$	$k_{30} = 4.67 \times 10^{-12} \left(\frac{T}{300}\right)^{-0.6}$ $= 1.23 \times 10^{-17} \left(\frac{T}{300}\right)^{2.49} \exp\left(\frac{21845.6}{T}\right)$ $= 9.62 \times 10^{-8} \left(\frac{T}{300}\right)^{-1.37} \exp\left(\frac{-115786.2}{T}\right)$	$T \leq 7950 \text{ K}$ $7950 \text{ K} < T \leq 21140 \text{ K}$ $T > 21140 \text{ K}$	24
31	$\text{Si}^+ + \text{e}^- \rightarrow \text{Si} + \gamma$	$k_{31} = 7.5 \times 10^{-12} \left(\frac{T}{300}\right)^{-0.55}$ $= 4.86 \times 10^{-12} \left(\frac{T}{300}\right)^{-0.32}$ $= 9.08 \times 10^{-14} \left(\frac{T}{300}\right)^{0.818}$	$T \leq 2000 \text{ K}$ $2000 \text{ K} < T \leq 10^4 \text{ K}$ $T > 10^4 \text{ K}$	25
32	$\text{O}^+ + \text{e}^- \rightarrow \text{O} + \gamma$	$k_{32} = 1.30 \times 10^{-10} T^{-0.64}$ $= 1.41 \times 10^{-10} T^{-0.66} + 7.4 \times 10^{-4} T^{-1.5}$ $\times \exp\left(-\frac{175000}{T}\right) [1.0 + 0.062 \times \exp\left(-\frac{145000}{T}\right)]$	$T \leq 400 \text{ K}$ $T > 400 \text{ K}$	26

Table 2—Continued

No.	Reaction	Rate coefficient (cm <sup>3</sup> s <sup>-1</sup> )	Ref.
33	$\text{C} + \text{e}^- \rightarrow \text{C}^+ + \text{e}^- + \text{e}^-$	$k_{33} = 6.85 \times 10^{-8} (0.193 + u)^{-1} u^{0.25} e^{-u}$	$u = 11.26/T_e$ 27
34	$\text{Si} + \text{e}^- \rightarrow \text{Si}^+ + \text{e}^- + \text{e}^-$	$k_{34} = 1.88 \times 10^{-7} (1.0 + u^{0.5})(0.376 + u)^{-1} u^{0.25} e^{-u}$	$u = 8.2/T_e$ 27
35	$\text{O} + \text{e}^- \rightarrow \text{O}^+ + \text{e}^- + \text{e}^-$	$k_{35} = 3.59 \times 10^{-8} (0.073 + u)^{-1} u^{0.34} e^{-u}$	$u = 13.6/T_e$ 27
36	$\text{O}^+ + \text{H} \rightarrow \text{O} + \text{H}^+$	$k_{36} = 4.99 \times 10^{-11} T^{0.405} + 7.54 \times 10^{-10} T^{-0.458}$	28
37	$\text{O} + \text{H}^+ \rightarrow \text{O}^+ + \text{H}$	$k_{37} = [1.08 \times 10^{-11} T^{0.517} + 4.00 \times 10^{-10} T^{0.00669}] \exp(-\frac{227}{T})$	29
38	$\text{O} + \text{He}^+ \rightarrow \text{O}^+ + \text{He}$	$k_{38} = 4.991 \times 10^{-15} \left(\frac{T}{10000}\right)^{0.3794} \exp\left(-\frac{T}{1121000}\right) + 2.780 \times 10^{-15} \left(\frac{T}{10000}\right)^{-0.2163} \exp\left(\frac{T}{815800}\right)$	30
39	$\text{C} + \text{H}^+ \rightarrow \text{C}^+ + \text{H}$	$k_{39} = 3.9 \times 10^{-16} T^{0.213}$	29
40	$\text{C}^+ + \text{H} \rightarrow \text{C} + \text{H}^+$	$k_{40} = 6.08 \times 10^{-14} \left(\frac{T}{10000}\right)^{1.96} \exp\left(-\frac{170000}{T}\right)$	29
41	$\text{C} + \text{He}^+ \rightarrow \text{C}^+ + \text{He}$	$k_{41} = 8.58 \times 10^{-17} T^{0.757}$ $= 3.25 \times 10^{-17} T^{0.968}$ $= 2.77 \times 10^{-19} T^{1.597}$	$T \leq 200 \text{ K}$ $200 < T \leq 2000 \text{ K}$ $T > 2000 \text{ K}$ 31
42	$\text{Si} + \text{H}^+ \rightarrow \text{Si}^+ + \text{H}$	$k_{42} = 5.88 \times 10^{-13} T^{0.848}$ $= 1.45 \times 10^{-13} T$	$T \leq 10^4 \text{ K}$ $T > 10^4 \text{ K}$ 32
43	$\text{Si} + \text{He}^+ \rightarrow \text{Si}^+ + \text{He}$	$k_{43} = 3.3 \times 10^{-9}$	33
44	$\text{C}^+ + \text{Si} \rightarrow \text{C} + \text{Si}^+$	$k_{44} = 2.1 \times 10^{-9}$	33
45	$\text{Si}^+ + \text{H}^+ \rightarrow \text{Si}^{++} + \text{H}$	$k_{45} = 4.10 \times 10^{-10} \left(\frac{T}{10000}\right)^{0.24} \times \left[1.0 + 3.17 \exp\left(\frac{T}{2.39 \times 10^6}\right)\right] \exp\left(-\frac{3.178}{T_e}\right)$	32
46	$\text{Si}^{++} + \text{H} \rightarrow \text{Si}^+ + \text{H}^+$	$k_{46} = 1.23 \times 10^{-9} \left(\frac{T}{10000}\right)^{0.24} \times \left[1.0 + 3.17 \exp\left(\frac{T}{2.39 \times 10^6}\right)\right]$	32
47	$\text{Si}^{++} + \text{e}^- \rightarrow \text{Si}^+ + \gamma$	$k_{47,\text{rr}} = 1.75 \times 10^{-12} \left(\frac{T}{10000}\right)^{-0.6346}$	34

Table 2—Continued

No.	Reaction	Rate coefficient ( $\text{cm}^3 \text{s}^{-1}$ )	Ref.
		$k_{47,\text{di}} = 2.2552 \times 10^{-11} T_e^{-1.5} \exp\left(-\frac{2.76}{T_e}\right)$ $+ 5.6058 \times 10^{-9} T_e^{-1.5} \exp\left(-\frac{10.13}{T_e}\right)$	35
75	$\text{H}_2 + \text{He} \rightarrow \text{H} + \text{H} + \text{He}$	$k_{75,\text{l}} = \text{dex}[-27.029 + 3.801 \log(T) - 29487/T]$ $k_{75,\text{h}} = \text{dex}[-2.729 - 1.75 \log(T) - 23474/T]$ $n_{\text{cr,He}} = \text{dex}[5.0792(1.0 - 1.23 \times 10^{-5}(T - 2000))]$	36
76	$\text{OH} + \text{H} \rightarrow \text{O} + \text{H} + \text{H}$	$k_{76} = 6.0 \times 10^{-9} \exp\left(-\frac{50900}{T}\right)$	33
77	$\text{HOC}^+ + \text{H}_2 \rightarrow \text{HCO}^+ + \text{H}_2$	$k_{77} = 3.8 \times 10^{-10}$	37
78	$\text{HOC}^+ + \text{CO} \rightarrow \text{HCO}^+ + \text{CO}$	$k_{78} = 4.0 \times 10^{-10}$	38
79	$\text{C} + \text{H}_2 \rightarrow \text{CH} + \text{H}$	$k_{79} = 6.64 \times 10^{-10} \exp\left(-\frac{11700}{T}\right)$	39
80	$\text{CH} + \text{H} \rightarrow \text{C} + \text{H}_2$	$k_{80} = 1.31 \times 10^{-10} \exp\left(-\frac{80}{T}\right)$	40
81	$\text{CH} + \text{H}_2 \rightarrow \text{CH}_2 + \text{H}$	$k_{81} = 5.46 \times 10^{-10} \exp\left(-\frac{1943}{T}\right)$	41
82	$\text{CH} + \text{C} \rightarrow \text{C}_2 + \text{H}$	$k_{82} = 6.59 \times 10^{-11}$	42
83	$\text{CH} + \text{O} \rightarrow \text{CO} + \text{H}$	$k_{83} = 6.6 \times 10^{-11}$ $= 1.02 \times 10^{-10} \exp\left(-\frac{914}{T}\right)$	$T \leq 2000 \text{ K}$ $T > 2000 \text{ K}$
84	$\text{CH}_2 + \text{H} \rightarrow \text{CH} + \text{H}_2$	$k_{84} = 6.64 \times 10^{-11}$	45
85	$\text{CH}_2 + \text{O} \rightarrow \text{CO} + \text{H} + \text{H}$	$k_{85} = 1.33 \times 10^{-10}$	46
86	$\text{CH}_2 + \text{O} \rightarrow \text{CO} + \text{H}_2$	$k_{86} = 8.0 \times 10^{-11}$	47
87	$\text{C}_2 + \text{O} \rightarrow \text{CO} + \text{C}$	$k_{87} = 5.0 \times 10^{-11} \left(\frac{T}{300}\right)^{0.5}$ $= 5.0 \times 10^{-11} \left(\frac{T}{300}\right)^{0.757}$	$T \leq 300 \text{ K}$ $T > 300 \text{ K}$
88	$\text{O} + \text{H}_2 \rightarrow \text{OH} + \text{H}$	$k_{88} = 3.14 \times 10^{-13} \left(\frac{T}{300}\right)^{2.7} \exp\left(-\frac{3150}{T}\right)$	50

Table 2—Continued

No.	Reaction	Rate coefficient (cm <sup>3</sup> s <sup>-1</sup> )	Ref.
89	OH + H → O + H <sub>2</sub>	$k_{89} = 6.99 \times 10^{-14} \left(\frac{T}{300}\right)^{2.8} \exp\left(-\frac{1950}{T}\right)$	51
90	OH + H <sub>2</sub> → H <sub>2</sub> O + H	$k_{90} = 2.05 \times 10^{-12} \left(\frac{T}{300}\right)^{1.52} \exp\left(-\frac{1736}{T}\right)$	52
91	OH + C → CO + H	$k_{91} = 1.0 \times 10^{-10}$	42
92	OH + O → O <sub>2</sub> + H	$k_{92} = 3.50 \times 10^{-11}$ $= 1.77 \times 10^{-11} \exp\left(\frac{178}{T}\right)$	$T \leq 261$ K 53 $T > 261$ K 41
93	OH + OH → H <sub>2</sub> O + H	$k_{93} = 1.65 \times 10^{-12} \left(\frac{T}{300}\right)^{1.14} \exp\left(-\frac{50}{T}\right)$	42
94	H <sub>2</sub> O + H → H <sub>2</sub> + OH	$k_{94} = 1.59 \times 10^{-11} \left(\frac{T}{300}\right)^{1.2} \exp\left(-\frac{9610}{T}\right)$	54
95	O <sub>2</sub> + H → OH + O	$k_{95} = 2.61 \times 10^{-10} \exp\left(-\frac{8156}{T}\right)$	41
96	O <sub>2</sub> + H <sub>2</sub> → OH + OH	$k_{96} = 3.16 \times 10^{-10} \exp\left(-\frac{21890}{T}\right)$	55
97	O <sub>2</sub> + C → CO + O	$k_{97} = 4.7 \times 10^{-11} \left(\frac{T}{300}\right)^{-0.34}$ $= 2.48 \times 10^{-12} \left(\frac{T}{300}\right)^{1.54} \exp\left(\frac{613}{T}\right)$	$T \leq 295$ K 42 $T > 295$ K 41
98	CO + H → C + OH	$k_{98} = 1.1 \times 10^{-10} \left(\frac{T}{300}\right)^{0.5} \exp\left(-\frac{77700}{T}\right)$	33
99	H <sub>2</sub> <sup>+</sup> + H <sub>2</sub> → H <sub>3</sub> <sup>+</sup> + H	$k_{99} = 2.24 \times 10^{-9} \left(\frac{T}{300}\right)^{0.042} \exp\left(-\frac{T}{46600}\right)$	56
100	H <sub>3</sub> <sup>+</sup> + H → H <sub>2</sub> <sup>+</sup> + H <sub>2</sub>	$k_{100} = 7.7 \times 10^{-9} \exp\left(-\frac{17560}{T}\right)$	57
101	C + H <sub>2</sub> <sup>+</sup> → CH <sup>+</sup> + H	$k_{101} = 2.4 \times 10^{-9}$	33
102	C + H <sub>3</sub> <sup>+</sup> → CH <sup>+</sup> + H <sub>2</sub>	$k_{102} = 2.0 \times 10^{-9}$	33
103	C <sup>+</sup> + H <sub>2</sub> → CH <sup>+</sup> + H	$k_{103} = 1.0 \times 10^{-10} \exp\left(-\frac{4640}{T}\right)$	58
104	CH <sup>+</sup> + H → C <sup>+</sup> + H <sub>2</sub>	$k_{104} = 7.5 \times 10^{-10}$	59
105	CH <sup>+</sup> + H <sub>2</sub> → CH <sub>2</sub> <sup>+</sup> + H	$k_{105} = 1.2 \times 10^{-9}$	59
106	CH <sup>+</sup> + O → CO <sup>+</sup> + H	$k_{106} = 3.5 \times 10^{-10}$	60

Table 2—Continued

No.	Reaction	Rate coefficient ( $\text{cm}^3 \text{s}^{-1}$ )	Ref.
107	$\text{CH}_2 + \text{H}^+ \rightarrow \text{CH}^+ + \text{H}_2$	$k_{107} = 1.4 \times 10^{-9}$	33
108	$\text{CH}_2^+ + \text{H} \rightarrow \text{CH}^+ + \text{H}_2$	$k_{108} = 1.0 \times 10^{-9} \exp\left(-\frac{7080}{T}\right)$	33
109	$\text{CH}_2^+ + \text{H}_2 \rightarrow \text{CH}_3^+ + \text{H}$	$k_{109} = 1.6 \times 10^{-9}$	61
110	$\text{CH}_2^+ + \text{O} \rightarrow \text{HCO}^+ + \text{H}$	$k_{110} = 7.5 \times 10^{-10}$	33
111	$\text{CH}_3^+ + \text{H} \rightarrow \text{CH}_2^+ + \text{H}_2$	$k_{111} = 7.0 \times 10^{-10} \exp\left(-\frac{10560}{T}\right)$	33
112	$\text{CH}_3^+ + \text{O} \rightarrow \text{HCO}^+ + \text{H}_2$	$k_{112} = 4.0 \times 10^{-10}$	62
113	$\text{C}_2 + \text{O}^+ \rightarrow \text{CO}^+ + \text{C}$	$k_{113} = 4.8 \times 10^{-10}$	33
114	$\text{O}^+ + \text{H}_2 \rightarrow \text{OH}^+ + \text{H}$	$k_{114} = 1.7 \times 10^{-9}$	63
115	$\text{O} + \text{H}_2^+ \rightarrow \text{OH}^+ + \text{H}$	$k_{115} = 1.5 \times 10^{-9}$	33
116	$\text{O} + \text{H}_3^+ \rightarrow \text{OH}^+ + \text{H}_2$	$k_{116} = 8.4 \times 10^{-10}$	64
117	$\text{OH} + \text{H}_3^+ \rightarrow \text{H}_2\text{O}^+ + \text{H}_2$	$k_{117} = 1.3 \times 10^{-9}$	33
118	$\text{OH} + \text{C}^+ \rightarrow \text{CO}^+ + \text{H}$	$k_{118} = 7.7 \times 10^{-10}$	33
119	$\text{OH}^+ + \text{H}_2 \rightarrow \text{H}_2\text{O}^+ + \text{H}$	$k_{119} = 1.01 \times 10^{-9}$	65
120	$\text{H}_2\text{O}^+ + \text{H}_2 \rightarrow \text{H}_3\text{O}^+ + \text{H}$	$k_{120} = 6.4 \times 10^{-10}$	66
121	$\text{H}_2\text{O} + \text{H}_3^+ \rightarrow \text{H}_3\text{O}^+ + \text{H}_2$	$k_{121} = 5.9 \times 10^{-9}$	67
122	$\text{H}_2\text{O} + \text{C}^+ \rightarrow \text{HCO}^+ + \text{H}$	$k_{122} = 9.0 \times 10^{-10}$	68
123	$\text{H}_2\text{O} + \text{C}^+ \rightarrow \text{HOC}^+ + \text{H}$	$k_{123} = 1.8 \times 10^{-9}$	68
124	$\text{H}_3\text{O}^+ + \text{C} \rightarrow \text{HCO}^+ + \text{H}_2$	$k_{124} = 1.0 \times 10^{-11}$	33

Table 2—Continued

No.	Reaction	Rate coefficient ( $\text{cm}^3 \text{s}^{-1}$ )	Ref.
125	$\text{H}_3\text{O}^+ + \text{Si} \rightarrow \text{H}_2\text{O} + \text{SiH}^+$	$k_{125} = 1.8 \times 10^{-9}$	33
126	$\text{O}_2 + \text{C}^+ \rightarrow \text{CO}^+ + \text{O}$	$k_{126} = 3.8 \times 10^{-10}$	61
127	$\text{O}_2 + \text{C}^+ \rightarrow \text{CO} + \text{O}^+$	$k_{127} = 6.2 \times 10^{-10}$	61
128	$\text{O}_2 + \text{CH}_2^+ \rightarrow \text{HCO}^+ + \text{OH}$	$k_{128} = 9.1 \times 10^{-10}$	61
129	$\text{O}_2^+ + \text{C} \rightarrow \text{CO}^+ + \text{O}$	$k_{129} = 5.2 \times 10^{-11}$	33
130	$\text{CO} + \text{H}_3^+ \rightarrow \text{HOC}^+ + \text{H}_2$	$k_{130} = 2.7 \times 10^{-11}$	69
131	$\text{CO} + \text{H}_3^+ \rightarrow \text{HCO}^+ + \text{H}_2$	$k_{131} = 1.7 \times 10^{-9}$	69
132	$\text{HCO}^+ + \text{C} \rightarrow \text{CO} + \text{CH}^+$	$k_{132} = 1.1 \times 10^{-9}$	33
133	$\text{HCO}^+ + \text{Si} \rightarrow \text{CO} + \text{SiH}^+$	$k_{133} = 1.6 \times 10^{-9}$	33
134	$\text{HCO}^+ + \text{H}_2\text{O} \rightarrow \text{CO} + \text{H}_3\text{O}^+$	$k_{134} = 2.5 \times 10^{-9}$	70
135	$\text{Si} + \text{H}_3^+ \rightarrow \text{SiH}^+ + \text{H}_2$	$k_{135} = 3.7 \times 10^{-9}$	33
136	$\text{SiH}^+ + \text{H} \rightarrow \text{Si}^+ + \text{H}_2$	$k_{136} = 1.9 \times 10^{-9}$	71
137	$\text{SiH}^+ + \text{H}_2\text{O} \rightarrow \text{Si} + \text{H}_3\text{O}^+$	$k_{137} = 8.0 \times 10^{-10}$	71
138	$\text{H}_2 + \text{He}^+ \rightarrow \text{He} + \text{H}_2^+$	$k_{138} = 7.2 \times 10^{-15}$	72
139	$\text{H}_2 + \text{He}^+ \rightarrow \text{He} + \text{H} + \text{H}^+$	$k_{139} = 3.7 \times 10^{-14} \exp\left(\frac{35}{T}\right)$	72
140	$\text{CH} + \text{H}^+ \rightarrow \text{CH}^+ + \text{H}$	$k_{140} = 1.9 \times 10^{-9}$	33
141	$\text{CH}_2 + \text{H}^+ \rightarrow \text{CH}_2^+ + \text{H}$	$k_{141} = 1.4 \times 10^{-9}$	33
142	$\text{CH}_2 + \text{He}^+ \rightarrow \text{C}^+ + \text{He} + \text{H}_2$	$k_{142} = 7.5 \times 10^{-10}$	33
143	$\text{C}_2 + \text{He}^+ \rightarrow \text{C}^+ + \text{C} + \text{He}$	$k_{143} = 1.6 \times 10^{-9}$	33

Table 2—Continued

No.	Reaction	Rate coefficient ( $\text{cm}^3 \text{s}^{-1}$ )	Ref.
144	$\text{OH} + \text{H}^+ \rightarrow \text{OH}^+ + \text{H}$	$k_{144} = 2.1 \times 10^{-9}$	33
145	$\text{OH} + \text{He}^+ \rightarrow \text{O}^+ + \text{He} + \text{H}$	$k_{145} = 1.1 \times 10^{-9}$	33
146	$\text{H}_2\text{O} + \text{H}^+ \rightarrow \text{H}_2\text{O}^+ + \text{H}$	$k_{146} = 6.9 \times 10^{-9}$	73
147	$\text{H}_2\text{O} + \text{He}^+ \rightarrow \text{OH} + \text{He} + \text{H}^+$	$k_{147} = 2.04 \times 10^{-10}$	74
148	$\text{H}_2\text{O} + \text{He}^+ \rightarrow \text{OH}^+ + \text{He} + \text{H}$	$k_{148} = 2.86 \times 10^{-10}$	74
149	$\text{H}_2\text{O} + \text{He}^+ \rightarrow \text{H}_2\text{O}^+ + \text{He}$	$k_{149} = 6.05 \times 10^{-11}$	74
150	$\text{O}_2 + \text{H}^+ \rightarrow \text{O}_2^+ + \text{H}$	$k_{150} = 2.0 \times 10^{-9}$	73
151	$\text{O}_2 + \text{He}^+ \rightarrow \text{O}_2^+ + \text{He}$	$k_{151} = 3.3 \times 10^{-11}$	75
152	$\text{O}_2 + \text{He}^+ \rightarrow \text{O}^+ + \text{O} + \text{He}$	$k_{152} = 1.1 \times 10^{-9}$	75
153	$\text{O}_2^+ + \text{C} \rightarrow \text{O}_2 + \text{C}^+$	$k_{153} = 5.2 \times 10^{-11}$	33
154	$\text{CO} + \text{He}^+ \rightarrow \text{C}^+ + \text{O} + \text{He}$	$k_{154} = 1.4 \times 10^{-9} \left(\frac{T}{300}\right)^{-0.5}$	76
155	$\text{CO} + \text{He}^+ \rightarrow \text{C} + \text{O}^+ + \text{He}$	$k_{155} = 1.4 \times 10^{-16} \left(\frac{T}{300}\right)^{-0.5}$	76
156	$\text{CO}^+ + \text{H} \rightarrow \text{CO} + \text{H}^+$	$k_{156} = 7.5 \times 10^{-10}$	77
157	$\text{C}^- + \text{H}^+ \rightarrow \text{C} + \text{H}$	$k_{157} = 2.3 \times 10^{-7} \left(\frac{T}{300}\right)^{-0.5}$	33
158	$\text{O}^- + \text{H}^+ \rightarrow \text{O} + \text{H}$	$k_{158} = 2.3 \times 10^{-7} \left(\frac{T}{300}\right)^{-0.5}$	33
159	$\text{He}^+ + \text{H}^- \rightarrow \text{He} + \text{H}$	$k_{159} = 2.32 \times 10^{-7} \left(\frac{T}{300}\right)^{-0.52} \exp\left(\frac{T}{22400}\right)$	78
160	$\text{H}_3^+ + \text{e}^- \rightarrow \text{H}_2 + \text{H}$	$k_{160} = 2.34 \times 10^{-8} \left(\frac{T}{300}\right)^{-0.52}$	79
161	$\text{H}_3^+ + \text{e}^- \rightarrow \text{H} + \text{H} + \text{H}$	$k_{161} = 4.36 \times 10^{-8} \left(\frac{T}{300}\right)^{-0.52}$	79

Table 2—Continued

No.	Reaction	Rate coefficient ( $\text{cm}^3 \text{s}^{-1}$ )	Ref.
162	$\text{CH}^+ + \text{e}^- \rightarrow \text{C} + \text{H}$	$k_{162} = 7.0 \times 10^{-8} \left(\frac{T}{300}\right)^{-0.5}$	80
163	$\text{CH}_2^+ + \text{e}^- \rightarrow \text{CH} + \text{H}$	$k_{163} = 1.6 \times 10^{-7} \left(\frac{T}{300}\right)^{-0.6}$	81
164	$\text{CH}_2^+ + \text{e}^- \rightarrow \text{C} + \text{H} + \text{H}$	$k_{164} = 4.03 \times 10^{-7} \left(\frac{T}{300}\right)^{-0.6}$	81
165	$\text{CH}_2^+ + \text{e}^- \rightarrow \text{C} + \text{H}_2$	$k_{165} = 7.68 \times 10^{-8} \left(\frac{T}{300}\right)^{-0.6}$	81
166	$\text{CH}_3^+ + \text{e}^- \rightarrow \text{CH}_2 + \text{H}$	$k_{166} = 7.75 \times 10^{-8} \left(\frac{T}{300}\right)^{-0.5}$	82
167	$\text{CH}_3^+ + \text{e}^- \rightarrow \text{CH} + \text{H}_2$	$k_{167} = 1.95 \times 10^{-7} \left(\frac{T}{300}\right)^{-0.5}$	82
168	$\text{CH}_3^+ + \text{e}^- \rightarrow \text{CH} + \text{H} + \text{H}$	$k_{168} = 2.0 \times 10^{-7} \left(\frac{T}{300}\right)^{-0.4}$	33
169	$\text{OH}^+ + \text{e}^- \rightarrow \text{O} + \text{H}$	$k_{169} = 6.3 \times 10^{-9} \left(\frac{T}{300}\right)^{-0.48}$	83
170	$\text{H}_2\text{O}^+ + \text{e}^- \rightarrow \text{O} + \text{H} + \text{H}$	$k_{170} = 3.05 \times 10^{-7} \left(\frac{T}{300}\right)^{-0.5}$	84
171	$\text{H}_2\text{O}^+ + \text{e}^- \rightarrow \text{O} + \text{H}_2$	$k_{171} = 3.9 \times 10^{-8} \left(\frac{T}{300}\right)^{-0.5}$	84
172	$\text{H}_2\text{O}^+ + \text{e}^- \rightarrow \text{OH} + \text{H}$	$k_{172} = 8.6 \times 10^{-8} \left(\frac{T}{300}\right)^{-0.5}$	84
173	$\text{H}_3\text{O}^+ + \text{e}^- \rightarrow \text{H} + \text{H}_2\text{O}$	$k_{173} = 1.08 \times 10^{-7} \left(\frac{T}{300}\right)^{-0.5}$	85
174	$\text{H}_3\text{O}^+ + \text{e}^- \rightarrow \text{OH} + \text{H}_2$	$k_{174} = 6.02 \times 10^{-8} \left(\frac{T}{300}\right)^{-0.5}$	85
175	$\text{H}_3\text{O}^+ + \text{e}^- \rightarrow \text{OH} + \text{H} + \text{H}$	$k_{175} = 2.58 \times 10^{-7} \left(\frac{T}{300}\right)^{-0.5}$	85
176	$\text{H}_3\text{O}^+ + \text{e}^- \rightarrow \text{O} + \text{H} + \text{H}_2$	$k_{176} = 5.6 \times 10^{-9} \left(\frac{T}{300}\right)^{-0.5}$	85
177	$\text{O}_2^+ + \text{e}^- \rightarrow \text{O} + \text{O}$	$k_{177} = 1.95 \times 10^{-7} \left(\frac{T}{300}\right)^{-0.7}$	86
178	$\text{CO}^+ + \text{e}^- \rightarrow \text{C} + \text{O}$	$k_{178} = 2.75 \times 10^{-7} \left(\frac{T}{300}\right)^{-0.55}$	87
179	$\text{HCO}^+ + \text{e}^- \rightarrow \text{CO} + \text{H}$	$k_{179} = 2.76 \times 10^{-7} \left(\frac{T}{300}\right)^{-0.64}$	88
180	$\text{HCO}^+ + \text{e}^- \rightarrow \text{OH} + \text{C}$	$k_{180} = 2.4 \times 10^{-8} \left(\frac{T}{300}\right)^{-0.64}$	88

Table 2—Continued

No.	Reaction	Rate coefficient (cm <sup>3</sup> s <sup>-1</sup> )	Ref.
181	$\text{HOC}^+ + \text{e}^- \rightarrow \text{CO} + \text{H}$	$k_{181} = 1.1 \times 10^{-7} \left(\frac{T}{300}\right)^{-1.0}$	33
182	$\text{SiH}^+ + \text{e}^- \rightarrow \text{Si} + \text{H}$	$k_{182} = 2.0 \times 10^{-7} \left(\frac{T}{300}\right)^{-0.5}$	33
183	$\text{H}^- + \text{C} \rightarrow \text{CH} + \text{e}^-$	$k_{183} = 1.0 \times 10^{-9}$	33
184	$\text{H}^- + \text{O} \rightarrow \text{OH} + \text{e}^-$	$k_{184} = 1.0 \times 10^{-9}$	33
185	$\text{H}^- + \text{OH} \rightarrow \text{H}_2\text{O} + \text{e}^-$	$k_{185} = 1.0 \times 10^{-10}$	33
186	$\text{C}^- + \text{H} \rightarrow \text{CH} + \text{e}^-$	$k_{186} = 5.0 \times 10^{-10}$	33
187	$\text{C}^- + \text{H}_2 \rightarrow \text{CH}_2 + \text{e}^-$	$k_{187} = 1.0 \times 10^{-13}$	33
188	$\text{C}^- + \text{O} \rightarrow \text{CO} + \text{e}^-$	$k_{188} = 5.0 \times 10^{-10}$	33
189	$\text{O}^- + \text{H} \rightarrow \text{OH} + \text{e}^-$	$k_{189} = 5.0 \times 10^{-10}$	33
190	$\text{O}^- + \text{H}_2 \rightarrow \text{H}_2\text{O} + \text{e}^-$	$k_{190} = 7.0 \times 10^{-10}$	33
191	$\text{O}^- + \text{C} \rightarrow \text{CO} + \text{e}^-$	$k_{191} = 5.0 \times 10^{-10}$	33
192	$\text{H}_2 + \text{H}^+ \rightarrow \text{H}_3^+ + \gamma$	$k_{192} = 1.0 \times 10^{-16}$	89
193	$\text{C} + \text{e}^- \rightarrow \text{C}^- + \gamma$	$k_{193} = 2.25 \times 10^{-15}$	90
194	$\text{C} + \text{H} \rightarrow \text{CH} + \gamma$	$k_{194} = 1.0 \times 10^{-17}$	91
195	$\text{C} + \text{H}_2 \rightarrow \text{CH}_2 + \gamma$	$k_{195} = 1.0 \times 10^{-17}$	91
196	$\text{C} + \text{C} \rightarrow \text{C}_2 + \gamma$	$k_{196} = 4.36 \times 10^{-18} \left(\frac{T}{300}\right)^{0.35} \exp\left(-\frac{161.3}{T}\right)$	92
197	$\text{C} + \text{O} \rightarrow \text{CO} + \gamma$	$k_{197} = 2.1 \times 10^{-19}$	$T \leq 300 \text{ K}$ 93
		$= 3.09 \times 10^{-17} \left(\frac{T}{300}\right)^{0.33} \exp\left(-\frac{1629}{T}\right)$	$T > 300 \text{ K}$ 94
198	$\text{C}^+ + \text{H} \rightarrow \text{CH}^+ + \gamma$	$k_{198} = 4.46 \times 10^{-16} T^{-0.5} \exp\left(-\frac{4.93}{T^{2/3}}\right)$	95

Table 2—Continued

No.	Reaction	Rate coefficient (cm <sup>3</sup> s <sup>-1</sup> )	Ref.
199	$\text{C}^+ + \text{H}_2 \rightarrow \text{CH}_2^+ + \gamma$	$k_{199} = 4.0 \times 10^{-16} \left(\frac{T}{300}\right)^{-0.2}$	96
200	$\text{C}^+ + \text{O} \rightarrow \text{CO}^+ + \gamma$	$k_{200} = 2.5 \times 10^{-18}$ $= 3.14 \times 10^{-18} \left(\frac{T}{300}\right)^{-0.15} \exp\left(\frac{68}{T}\right)$	$T \leq 300 \text{ K}$ 93 $T > 300 \text{ K}$
201	$\text{O} + \text{e}^- \rightarrow \text{O}^- + \gamma$	$k_{201} = 1.5 \times 10^{-15}$	33
202	$\text{O} + \text{H} \rightarrow \text{OH} + \gamma$	$k_{202} = 9.9 \times 10^{-19} \left(\frac{T}{300}\right)^{-0.38}$	33
203	$\text{O} + \text{O} \rightarrow \text{O}_2 + \gamma$	$k_{203} = 4.9 \times 10^{-20} \left(\frac{T}{300}\right)^{1.58}$	91
204	$\text{OH} + \text{H} \rightarrow \text{H}_2\text{O} + \gamma$	$k_{204} = 5.26 \times 10^{-18} \left(\frac{T}{300}\right)^{-5.22} \exp\left(-\frac{90}{T}\right)$	97
205	$\text{Si}^+ + \text{H} \rightarrow \text{SiH}^+ + \gamma$	$k_{205} = 1.17 \times 10^{-17} \left(\frac{T}{300}\right)^{-0.14}$	98
206	$\text{H} + \text{H} + \text{H} \rightarrow \text{H}_2 + \text{H}$	$k_{206} = 1.32 \times 10^{-32} \left(\frac{T}{300}\right)^{-0.38}$ $= 1.32 \times 10^{-32} \left(\frac{T}{300}\right)^{-1.0}$	$T \leq 300 \text{ K}$ 99 $T > 300 \text{ K}$ 100
207	$\text{H} + \text{H} + \text{H}_2 \rightarrow \text{H}_2 + \text{H}_2$	$k_{207} = 2.8 \times 10^{-31} T^{-0.6}$	101
208	$\text{H} + \text{H} + \text{He} \rightarrow \text{H}_2 + \text{He}$	$k_{208} = 6.9 \times 10^{-32} T^{-0.4}$	102
209	$\text{C} + \text{C} + \text{M} \rightarrow \text{C}_2 + \text{M}$	$k_{209} = 5.99 \times 10^{-33} \left(\frac{T}{5000}\right)^{-1.6}$ $= 5.99 \times 10^{-33} \left(\frac{T}{5000}\right)^{-0.64} \exp\left(\frac{5255}{T}\right)$	$T \leq 5000 \text{ K}$ 103 $T > 5000 \text{ K}$ 104
210	$\text{C} + \text{O} + \text{M} \rightarrow \text{CO} + \text{M}$	$k_{210} = 6.16 \times 10^{-29} \left(\frac{T}{300}\right)^{-3.08}$ $= 2.14 \times 10^{-29} \left(\frac{T}{300}\right)^{-3.08} \exp\left(\frac{2114}{T}\right)$	$T \leq 2000 \text{ K}$ 105 $T > 2000 \text{ K}$ 76
211	$\text{C}^+ + \text{O} + \text{M} \rightarrow \text{CO}^+ + \text{M}$	$k_{211} = 100 \times k_{210}$	76
212	$\text{C} + \text{O}^+ + \text{M} \rightarrow \text{CO}^+ + \text{M}$	$k_{212} = 100 \times k_{210}$	76
213	$\text{O} + \text{H} + \text{M} \rightarrow \text{OH} + \text{M}$	$k_{213} = 4.33 \times 10^{-32} \left(\frac{T}{300}\right)^{-1.0}$	51
214	$\text{OH} + \text{H} + \text{M} \rightarrow \text{H}_2\text{O} + \text{M}$	$k_{214} = 2.56 \times 10^{-31} \left(\frac{T}{300}\right)^{-2.0}$	105

Table 2—Continued

No.	Reaction	Rate coefficient ( $\text{cm}^3 \text{s}^{-1}$ )	Ref.
215	$\text{O} + \text{O} + \text{M} \rightarrow \text{O}_2 + \text{M}$	$k_{215} = 9.2 \times 10^{-34} \left(\frac{T}{300}\right)^{-1.0}$	45
216	$\text{O} + \text{CH} \rightarrow \text{HCO}^+ + \text{e}^-$	$k_{216} = 2.0 \times 10^{-11} \left(\frac{T}{300}\right)^{0.44}$	106

References. — 1: Wishart (1979), 2: Launay et al. (1991), 3: Ramaker & Peek (1976), 4: Karpas, Anicich & Huntress (1979), 5: Moseley et al. (1970), 6: Schneider et al. (1994), 7: Savin et al. (2004), 8: Stibbe & Tennyson (1999), 9: Mac Low & Shull (1986), 10: Lepp & Shull (1983), 11: Martin, Keogh & Mandy (1998), 12: Shapiro & Kang (1987), 13: Janev et al. (1987), 14: Ferland et al. (1992), 15: Poulaert et al. (1978), 16: Savin (2002), 17: Gerlich (1982), 18: Mielke et al. (1994), 19: Shavitt (1959), 20: Hummer & Storey (1998), 21: Aldrovandi & Pequignot (1973), 22: Zygelman *et al.* (1989), 23: Kimura et al. (1993), 24: Nahar & Pradhan (1997), 25: Nahar (2000), 26: Nahar (1999), 27: Voronov (1997), 28: Stancil et al. (1999), 29: Stancil et al. (1998), 30: Zhao *et al.* (2004), 31: Kimura et al. (1993), 32: Kingdon & Ferland (1996), 33: Le Teuff, Millar & Markwick (2000), 34: Nahar (1995, 1996), 35: Mazzotta et al. (1998), 36: Dove et al. (1987), 37: Smith et al. (2002), 38: Wagner-Redeker et al. (1985), 39: Dean, Davidson & Hanson (1991), 40: Harding, Guadagnini & Schatz (1993), 41: Fit by Le Teuff, Millar & Markwick (2000) to data from the NIST chemical kinetics database; original source or sources unclear, 42: Smith, Herbst & Chang (2004), 43: Baulch et al. (1992), 44: Murrell & Rodriguez (1986), 45: Warnatz (1984), 46: Frank (1986), 47: Fit by Le Teuff, Millar & Markwick (2000) to data from Frank & Just (1984) and Frank, Bhaskaran & Just (1988), 48: Mitchell & Deveau (1983), 49: Fairbairn (1969) and paper III, 50: Natarajan & Roth (1987), 51: Tsang & Hampson (1986), 52: Oldenborg et al. (1992), 53: Carty et al. (2006) and paper III, 54: Cohen & Westberg (1979), 55: Azatyan, Aleksandrov & Troshin (1975), 56: Linder, Janev & Botero (1995), 57: Sidhu, Miller & Tennyson (1992), 58: Adams, Smith & Millar (1984), 59: McEwan et al. (1999), 60: Viggiano et al. (1980), 61: Smith & Adams (1977a,b), 62: Fehsenfeld (1976), 63: Smith, Adams & Miller (1978); Adams, Smith & Paulson (1980), 64: Milligan & McEwan (2000), 65: Jones, Birkinshaw & Twiddy (1981), 66: Raksit & Warneck (1980), 67: Kim, Theard & Huntress

(1974); Anicich et al. (1975), 68: Anicich, Huntress & Futrell (1976); Watson, Anicich & Huntress (1976), 69: Kim, Theard & Huntress (1975), 70: Adams, Smith & Grief (1978), 71: Herbst et al. (1989), 72: Barlow (1984), 73: Smith, Spanel & Mayhew (1992), 74: Mauclore, Deraï & Marx (1978a,b), 75: Adams & Smith (1976a,b), 76: Petuchowski et al. (1989), 77: Federer et al. (1984a,b), 78: Peart & Hayton (1994) 79: Fit by Woodall et al. (2007) to data from McCall et al. (2004), 80: Takagi, Kosugi, & Le Dourneuf (1991), 81: Larson et al. (1998), 82: Mitchell (1990), 83: Guberman (1995), 84: Rosén et al. (2000), 85: Jensen et al. (2000), 86: Alge, Adams & Smith (1983), 87: Rosén et al. (1998), 88: Geppert et al. (2005), 89: Gerlich & Horning (1992), 90: Stancil & Dalgarno (1998), 91: Prasad & Huntress (1980), 92: Andreazza & Singh (1997), 93: Dalgarno, Du & You (1990), 94: Singh et al. (1999), 95: Barinovs & van Hemert (2006), 96: Herbst (1985), 97: Field, Adams & Smith (1980), 98: Stancil et al. (2000), 99: Orel (1987), 100: Abel, Bryan, & Norman (2002) 101: Cohen & Westberg (1983), 102: Walkauskas & Kaufman (1975), 103: Paper III, 104: Fit by Le Teuff, Millar & Markwick (2000) to data from Fairbairn (1969) and Slack (1976), 105: Baulch et al. (1992), 106: MacGregor & Berry (1973)

Note. —  $T$  and  $T_e$  are the gas temperature in units of K and eV respectively. References are to the primary source of data for each reaction.

Table 3. List of processes in our thermal model.

Process	References
<b>Cooling:</b>	
Lyman- $\alpha$ cooling	Cen (1992)
He electronic excitation	Cen (1992); Bray et al. (2000)
Thermal bremsstrahlung	Shapiro & Kang (1987)
Compton cooling	Cen (1992)
H <sub>2</sub> rotational, vibrational lines	Le Bourlot et al. (1999)
HD rotational, vibrational lines	Lipovka, Núñez-López, & Avila-Reese (2005)
Fine structure lines (C, C <sup>+</sup> , O, Si, Si <sup>+</sup> )	Many sources; see Paper I
CO rotational, vibrational lines	Neufeld & Kaufman (1993); Neufeld, Lepp & Melnick (1995)
H <sub>2</sub> O rotational, vibrational lines	Neufeld & Kaufman (1993); Neufeld, Lepp & Melnick (1995)
OH rotational, vibrational lines lines	Pavlovski et al. (2002)
H <sup>+</sup> recombination	Ferland et al. (1992)
He <sup>+</sup> recombination	Aldrovandi & Pequignot (1973); Hummer & Storey (1998)
H & He collisional ionization	Janev et al. (1987)
H <sub>2</sub> collisional dissociation	See §2
<b>Heating:</b>	
H <sub>2</sub> gas-phase formation	Many sources; see Paper I and §2